CORROSION STUDIES OF CARBON STEEL, COPPER, AND TITANIUM AS WASTE PACKAGE MATERIALS

Prepared for

U.S. Nuclear Regulatory Commission
Contract NRC–HQ–12–C–02–0089

Prepared by

Xihua He[1]
Tae Ahn[2]

[1]Center for Nuclear Waste Regulatory Analyses
San Antonio, Texas

[2]U.S. Nuclear Regulatory Commission
Washington, DC

April 2019

EXECUTIVE SUMMARY

This study evaluates the corrosion resistance of three candidate waste package materials for high level radioactive waste (HLW) containment in deep geologic repositories. Carbon steel and copper (Cu) are two of the candidate waste container materials because their corrosion rates can be very low in anoxic water. However, absorption of hydrogen generated from the corrosion process into carbon steel could induce cracking. Likewise, species in the groundwater such as hydrogen sulfide and chloride ions could change the thermodynamic stability and electrochemical properties of Cu, especially its corrosion resistance. Titanium (Ti) is one of the candidate waste package materials for waste disposal in salt formations because of its wide passivity range. However, the presence of brine in salt formations could compromise the passivity of Ti at elevated temperatures, leading to localized corrosion and hydrogen induced cracking. This study (i) investigated the possibility of hydrogen induced cracking of carbon steel under static loading in simulated granitic groundwater, (ii) evaluated Cu corrosion in simulated granitic groundwater and evaluated the effects of Cl^- on Cu corrosion at 50 °C [122 °F] in solutions with varying Cl^- concentration and extremely low O_2, and (iii) evaluated Ti passivity, localized corrosion resistance, and hydrogen induced cracking in brine.

Cathodic charging was applied to carbon steel under static loading condition in simulated granitic groundwater over a temperature range of 20–80°C [68–176 °F] to investigate hydrogen induced cracking. The test duration was up to 3 months. In one test, the solution was acidified to pH 2, and in another test the exposure surface was creviced to enhance hydrogen entry. Hydrogen (H_2) bubbles and hydroxides were observed to be formed on the exposure surface under cathodic charging condition. However, cracking was not observed in any of the charged specimens. Similar to the high cracking resistance observed under alkaline conditions in previous work, carbon steel also showed high cracking resistance under static loading in acidified simulated granitic groundwater.

In simulated granitic groundwater and in another four solutions with different Cl^- concentrations, Cu corrosion potential (E_{corr}) reached steady state values in a couple of days. Consistent with previous observation, E_{corr} decreased with logarithmic Cl^- concentration, and exchange current density obtained from potentiodynamic polarization increased with Cl^- concentration. Electrochemical impedance spectroscopy (EIS) indicated that Cu corrosion formed films on the exposed surface; the film structure, thickness, and properties varied depending on the solution composition. Mass transport likely controls the Cu corrosion process. The Cu corrosion properties correlate well with Cl^- concentration. The re-evaluation corroborates the previous observation that Cl^- plays a significant role in enhancing corrosion of Cu in solutions with extremely low O_2 concentrations. Higher Cl^- concentration could have depolarized the anodic reaction, resulting in lower E_{corr} values and potentially higher corrosion rates.

Ti Grades 2, 7, and 29 were selected to represent Ti materials with different alloy elements and microstructures. Ti Grade 2 was selected as a baseline material for comparison because of its lack of any alloying element. Ti Grade 7 has palladium (Pd) added to ennoble the material, but it is also a single α-phase Ti as Ti Grade 2. Ti Grade 29 has Al, V, and Ru added and it is an α plus β-phase Ti material. E_{corr} monitoring and EIS were performed to study material passivity. Crevice corrosion tests were performed to study localized corrosion susceptibility. Cathodic charging was performed to evaluate hydrogen induced cracking resistance. A synthetic brine with composition similar to naturally occurring brines from the reservoirs in the Castile Formation near the Waste Isolation Pilot Plant (WIPP) site was used in the tests of Ti. Ti Grade 7 showed high passivity and negligible general corrosion in brines up to the highest temperature of 180 °C [356 °F] used in this study. Ti Grade 7 also exhibited high crevice corrosion resistance and very low hydrogen absorption efficiency, even in an acidified solution

with pH 2. Ti Grade 2 showed a similar level of general corrosion resistance as Ti Grade 7 at 80 °C [176 F], but it is susceptible to crevice corrosion, possibly because it does not contain any noble alloying element. Ti Grade 29 showed lower passivity in the same solution compared to Ti Grades 2 and 7 at 80 °C [176 °F], possibly because of its two-phase microstructure. Because of time constraints, limited studies were performed on Ti Grades 2 and 29. Further work is needed provide a more complete characterization of the corrosion properties of different Ti alloys as candidate waste package materials for a repository in a salt formation.

CONTENTS

Section Page

EXECUTIVE SUMMARY ii
FIGURES v
TABLES vii
ABBREVIATIONS/ACRONYMS viii
ACKNOWLEDGMENTS ix

1 INTRODUCTION 1-1

2 EXPERIMENTAL APPROACHES 2-1
2.1 Hydrogen Induced Cracking of Carbon Steel under Static Load 2-1
2.2 Effects of Chloride on Copper Corrosion 2-1
2.2.1 Cu and test solution 2-1
2.2.2 Electrochemical methods 2-1
2.3 Titanium Corrosion in Brine 2-3
2.3.1 Test materials and solution 2-3
2.3.2 Electrochemical methods 2-3

3 EXPERIMENTAL RESULTS AND DISCUSSION 3-1
3.1 Hydrogen Induced Cracking of Carbon Steel under Static Load 3-1
3.2 Effects of Chloride on Copper Corrosion 3-2
3.2.1 Corrosion potential (E_{corr}) 3-2
3.2.2 Potentiodynamic polarization 3-2
3.2.3 Electrochemical Impedance Spectroscopy 3-7
3.2.4 Discussion 3-13
3.3 Titanium Corrosion in Brine 3-15
3.3.1 Titanium Grade 7 3-15
3.3.1.1 Corrosion potential in aerated brine 3-15
3.3.1.2 Electrochemical impedance spectroscopy in aerated brine 3-16
3.3.1.3 Crevice corrosion in aerated brine 3-18
3.3.1.4 Cyclic potentiodynamic polarization in N_2 deaerated brine 3-18
3.3.1.5 Cathodic charging in N_2 deaerated brine 3-22
3.3.2 Titanium Grade 2 3-24
3.3.2.1 Corrosion potential in aerated brine 3-24
3.3.2.2 Electrochemical impedance spectroscopy in aerated brine 3-24
3.3.2.3 Crevice corrosion experiments exposed to aerated brine 3-24
3.3.2.4 Cyclic potentiodynamic polarization in N_2 deaerated brine 3-24
3.3.3 Titanium Grade 29 3-27
3.3.4 Discussion 3-28

4 SUMMARY 4-1

5 REFERENCES 5-1

FIGURES

Figure Page

2-1 Schematics in evaluating effects of chloride on copper corrosion....2-2

3-1 (a) Cathodic charging potential and current of carbon steel in simulated granitic groundwater at 20 °C [68 °F] and (b) post-charging carbon steel U-bend apex 3-2
3-2 Cathodic charging potential and current at 50 °C [122 °F] and post-charging carbon steel specimens in (a) simulated granitic groundwater and (b) acidified simulated granitic groundwater 3-3
3-3 Cathodic charging potential and current at 80 °C and post-charging carbon steel specimens (a) U-bend apex was exposed to solution and (b) U-bend apex was covered with Microstop™ paint as crevice former 3-4
3-4 (a) E_{corr} of Cu as a function of time in five solutions with varying Cl^- concentration at 50 °C [122 °F], and (b) relatively steady E_{corr} at the end of each test as a function of Cl^- concentration....3-5
3-5 Cyclic voltammograms on copper in five solutions at 50 °C [122 °F] (a) forward and backward scans, (b) forward scan, and (c) backward scan 3-6
3-6 Tafel regions and the fit to Tafel equation for the data in forward scan (a) region 1 and (b) region 2 in Figure 3-4(b)....3-8
3-7 EIS of Cu exposed to Solution 1 at 50 °C [122 °F] (2×10^3 ppm SO_4^{2-}) at 6, 12, 18, and 24 days; (a) Nyquist plot and (b) Bode plot....3-9
3-8 EIS of Cu exposed to Solution 2 (2×10^3 ppm SO_4^{2-} and 1×10^3 ppm Cl^-) at 50 °C [122 °F] at 8, 14, 20, and 26 days; (a) Nyquist plot and (b) Bode plot 3-9
3-9 EIS of Cu exposed to Solution 3 (2×10^3 ppm SO_4^{2-} and 1×10^4 ppm Cl^-) at 50 °C [122 °F] at 7, 22, and 29 days; (a) Nyquist plot and (b) Bode plot 3-10
3-10 EIS of Cu exposed to Solution 4 (2×10^3 ppm SO_4^{2-} and 1×10^5 ppm Cl^-) at 50 °C [122 °F] at 8, 14, 20, and 26 days at 50 °C [122 °F]; (a) Nyquist plot and (b) Bode plot....3-10
3-11 EIS of Cu exposed to simulated granitic groundwater at 50 °C [122 °F] at 7, 14, 20, and 26 days at 50 °C [122 °F]; (a) Nyquist plot and (b) Bode plot 3-11
3-12 (a) Two- and (b) three-time constant circuits used to model the EIS data in Figures 3-7 through 3-11....3-11
3-13 Averaged (a) polarization resistance, (b) corrosion rate, (c) double layer capacitance, and (d) solution resistance of Cu exposed to five solutions at 50 °C [122 °F] derived by fitting the equivalent-circuit model in Figures 3-12(a) to the EIS data 3-14
3-14 Effect of increasing Cl^- concentration on the E_{corr} and corrosion tendency....3-15
3-15 (a) E_{corr} of Ti Grade 7 as a function of time at temperatures of 80 °C [176 °F], 100 °C [212 °F], 120 °C [248 °F], 140 °C [284 °F], 160 °C [320 °F], and 180 °C [356 °F] and (b) cylindrical electrode after testing from 100 °C [212 °F] to 180 °C [356 °F] for about 45 days 3-16
3-16 EIS of Ti Grade 7 exposed to brine (a) Nyquist plot and (b) Bode plot at 80 °C [176 °F] at 6, 12, 18, 24, and 30 days, (c) Nyquist plot, and (d) Bode plot at 120 °C [248 °F] and 150 °C [302 °F]....3-17
3-17 Randles circuit used to fit the EIS data in low frequency region in Figure 3-16 3-18
3-18 Crevice corrosion current and potential of Ti Grade 7 at (a) 80 °C [176 °F] and (b) 140 °C [284 °F] in brine 3-19

FIGURES (Continued)

Figure Page

3-19 Cyclic potentiodynamic polarization of Ti Grade 7 in N_2 deaerated brine (a) 80 °C [176 °F], (b) 95 °C [203 °F], (c) 120 °C [248 °F], (d) 140 °C [284 °F], (e)160 °C [320 °F], and (f) 180 °C [356 °F]; (g) forward scan and (h) reverse scan 3-20

3-20 Ti Grade 7 coupons after cyclic potentiodynamic polarization in N_2 deaerated brine (a) 80 °C [176 °F], (b) 95 °C [203 °F], (c) 120 °C [248 °F], (d) 140 °C [284 °F], (e)160 °C [320 °F], and (f) 180 °C [356 °F] 3-21

3-21 Cathodic charging potential and current and post-charging Ti Grade 7 specimens in brine at 50 °C [122 °F] (a) 1st test and (b) 2nd test 3-23

3-22 E_{corr} of Ti Grade 2 as a function of time in brine at 80 °C [176 °F] 3-25

3-23 EIS of Ti Grade 2 exposed to brine at 80 °C [176 °F] at 1, 6, 12, 18, and 24 days (a) Nyquist plot and (b) Bode plot 3-25

3-24 Crevice corrosion current and potential of Ti Grade 2 in coupling to Ti Grade 7 at (a) 80 °C [176 °F], (b) 95 °C [203 °F], and (c) 140 °C [284 °F] in brine 3-26

3-25 Cyclic potentiodynamic polarization of Ti Grade 2 in N_2 deaerated brine (a) 80 °C [176 °F], (b) repeating test at 80 °C [176 °F], (c) repeating test at 80 °C [176 °F] up to 8 V_{SCE} and the posttest specimen, (d) forward scan, and (e) reverse scan 3-27

3-26 Cyclic potentiodynamic polarization of Ti Grade 29 in N_2 deaerated brine at 80 °C [176 °F] in comparing to Ti Grades 2 and 7 3-28

3-27 Cathodic charging potential and current of Ti Grade 29 specimen in brine at 50 °C [122 °F] 3-28

3-28 Schematic illustrating the polarization curve for Ti and its relationship to the cathodic polarization curves for proton reduction on Ti Grade 2 and on a Ti alloy containing a catalytic alloying element such as Pd 3-29

TABLES

Table		Page
2-1	Chemical formula of simulated granitic groundwater for hydrogen induced cracking tests of carbon steel	2-2
2-2	Solution composition evaluating effects of chloride on Cu corrosion at 50 °C [122 °F]	2-2
2-3	Chemical formula of brine for corrosion tests of titanium	2-3
2-4	Electrochemical methods to assess titanium corrosion	2-4
3-1	Tafel slopes and exchange current density for anodic polarization of copper at 50 °C [122 °F]	3-8
3-2	Corrosion parameters and corrosion rates at 50 °C [122 °F] derived by fitting equivalent circuits to the EIS data	3-12
3-3	Corrosion parameters and corrosion rates of Ti Grade 7 derived by fitting EIS to Randles circuit	3-19
3-4	Hydrogen concentration analysis of Ti Grade 7 subject to cathodic charging	3-23
3-5	Corrosion parameters and corrosion rates of Ti Grade 2 derived by fitting EIS to the Randles equivalent circuit	3-26

ABBREVIATION/ACRONYMS

Al	aluminum
$CaCl_2$	calcium chloride
Cl^-	chloride
CNWRA®	Center for Nuclear Waste Regulatory Analyses
CPE_f	constant phase element of film
CPE_{dl}	constant phase element of double layer
Cu	copper
E_{corr}	corrosion potential
EIS	electrochemical impedance spectroscopy
FY	fiscal year
HLW	high-level radioactive waste
HS^-	hydrogen sulfide ion
KCl	potassium chloride
$MgCl_2 \cdot 6H_2O$	magnesium chloride hexahydrate
NaBr	sodium bromide
Na_2SO_4	sodium sulfate
NaCl	sodium chloride
$NaHCO_3$	sodium bicarbonate
Pd	palladium
R_f	film resistance
R_p	polarization resistance
R_s	solution resistance
Ru	ruthenium
Ti	titanium
NRC	U.S. Nuclear Regulatory Commission
V	vanadium

ACKNOWLEDGMENTS

This report was prepared to document work performed by the Center for Nuclear Waste Regulatory Analyses (CNWRA®) for the U.S. Nuclear Regulatory Commission (NRC) under Contract No. 31310018D0001. The activities reported here were performed on behalf of the NRC Office of Nuclear Material Safety and Safeguards, Division of Spent Fuel Management. The report is an independent product of CNWRA and does not necessarily reflect the views or regulatory position of NRC. The NRC staff views expressed herein are preliminary and do not constitute a final judgment or determination of the matters addressed or of the acceptability of any licensing action that may be under consideration at NRC.

The authors acknowledge the valuable contributions of the NRC Project Manager, J. Gwo, for guidance, feedback, and information provided over the duration of this project. Comments from C. Markley also helped improve the report.

The authors thank B. Werling for support in achieving stable and inert atmospheric conditions in the glovebox used in conducting the tests reported herein, O. Pensado for technical review, and W. Patrick for programmatic review. The authors also thank A. Ramos for support in report preparation.

QUALITY OF DATA, ANALYSES, AND CODE DEVELOPMENT

DATA: All CNWRA-generated original data contained in this report meet the quality assurance requirements described in the CNWRA Quality Assurance Manual and supporting procedures. Sources for other data should be consulted for determining the level of quality for those data. Scientific Notebook 1312 (He, 2018) documents experimental conditions.

ANALYSES AND CODES: No software subject to control under Technical Operating Procedure TOP-018 was used in this study.

REFERENCES:

He, X. “Copper and Carbon Steel Experiments.” Scientific Notebook 1312.
San Antonio, Texas: Center for Nuclear Waste Regulatory Analyses. pp. 1–88. 2019.

1 INTRODUCTION

Many countries have been exploring the feasibility of high-level radioactive waste (HLW) disposal in deep geologic repositories, including Canada, Finland, Germany, Japan, Sweden, and Switzerland (King, 2013). Carbon steel and copper (Cu) are two of the candidate metallic materials for waste containment in deep geologic repository and some titanium (Ti) alloys are candidate materials for waste containment in salt formations. After tens or hundreds of years, the chemical environment around the waste containers in the potential deep repositories is generally expected to evolve from oxic to anoxic conditions. Under certain conditions, corrosion rates of carbon steel and Cu could be sufficiently slow that these waste containers could isolate the HLW for a very long time. However, hydrogen produced from cathodic reaction accompanying carbon steel corrosion may be absorbed into the material and induce cracking, which can shorten the lifetime of the container. Likewise, species in the groundwater such as chloride (Cl^-) and hydrogen sulfide (HS^-) ions could change Cu thermodynamic and chemical stability and corrosion resistance. Ti alloys are known for their high passivity even under very corrosive conditions; however, the brines associated with salt formations can depassivate the material, leading to localized corrosion and hydrogen induced cracking. Furthermore, elevated temperatures induced by HLW decay heat release also could affect these material properties of Ti alloys.

Previous work (He and Ahn, 2017a) showed that carbon steel is resistant to hydrogen induced cracking in alkaline solutions. He and Ahn (2018) evaluated the effects of Cl^- on Cu corrosion over a concentration range from 0 to 10^5 ppm Cl^- with extremely low O_2 concentrations at 50 °C [122 °F]. The study showed that Cl^- enhanced Cu corrosion in these solutions. The work reported here continued to evaluate the corrosion properties of some candidate waste package materials, particularly carbon steel, Cu, and Ti, at different temperatures and in a variety of chemical solutions. The research objectives were to (i) examine the possibility of hydrogen induced cracking of carbon steel under static loading in simulated granitic groundwater; (ii) evaluate Cu corrosion in simulated granitic groundwater and repeat the evaluation of the effects of Cl^- on Cu corrosion at 50 °C [122 °F] to corroborate the results in He and Ahn (2018); and (iii) evaluate Ti passivity, localized corrosion resistance, and hydrogen induced cracking in brine.

2 EXPERIMENTAL APPROACHES

Carbon steel, Copper (Cu), and titanium (Ti) are the three waste package materials evaluated in this study under various chemical solutions and temperature ranges. The materials, solutions, and experimental methods are described in this chapter.

2.1 Hydrogen Induced Cracking of Carbon Steel under Static Load

Previous studies of carbon steel evaluated its corrosion resistance and hydrogen induced cracking mainly in simulated concrete pore water (He and Ahn, 2017a,b; He et al., 2015). This study focused only on evaluating hydrogen induced cracking resistance in simulated granitic groundwater with lower pH compared to concrete pore water. The commonly used A516 Grade 60 carbon steel (UNS K02100), which is the same material as in previous work (He and Ahn, 2017a,b; He et al., 2015), was used in the test. The apex of the U-bend under static loading was charged cathodically in simulated granitic groundwater with the composition shown in Table 2-1, which is the same solution used in He and Ahn (2017b) and He et al. (2015). The solution composition is based on reference Canadian Shield groundwater compositions that are described in He et al. (2015). Chemical reagents including sodium chloride (NaCl), potassium chloride (KCl), sodium sulfate (Na_2SO_4), calcium chloride ($CaCl_2$), magnesium chloride hexahydrate ($MgCl_2 \cdot 6H_2O$), and sodium bicarbonate ($NaHCO_3$) were used to prepare this simulated granitic groundwater. The pH was measured to be 6.65 at ambient temperature and pressure before the test. During the test, the solution was deaerated with N_2.

2.2 Effects of Chloride on Copper Corrosion

2.2.1 Cu and test solution

Oxygen-free high conductivity Cu cylindrical electrodes were fabricated from the same batch of material used in all previous work (He et al., 2015; He and Ahn, 2017a,b; He and Ahn, 2018). The tests were conducted in simulated granitic groundwater with the composition shown in Table 2-1 and four other solutions with varying Cl^- concentration at 50 °C [122 °F]. The four other solutions were exactly the same as in He and Ahn (2018). The compositions are described in Table 2-2. For these four solutions, the SO_4^{2-} concentration was kept constant at 2×10^3 ppm by adding Na_2SO_4. The Cl^- concentration was varied from 0 to 1×10^3, 1×10^4, and 1×10^5 ppm by adding a constant amount of $CaCl_2$ (except for the zero Cl^- solution), and a varying amount of NaCl. The Cl^- concentration of the simulated granitic groundwater was between the solutions with 1×10^3 and 1×10^4 ppm Cl^- concentration. All the tests of Cu were conducted in a Labconco® controlled atmosphere glovebox, which provided a leak tight and inert atmosphere. This same glovebox was used for the fiscal year (FYs) 2017 and 2018 work reported in He and Ahn (2018, 2017a). The O_2 concentration in the solutions was about 0.1–0.2 ppb.

2.2.2 Electrochemical methods

Figure 2-1 illustrates the procedure for evaluating effects of chloride on Cu corrosion. Corrosion potential (E_{corr}) monitoring, electrochemical impedance spectroscopy (EIS), and cyclic potentiodynamic polarization were used to evaluate the effects of chloride on Cu corrosion. The E_{corr} was monitored and EIS data were collected after several days of E_{corr} monitoring. EIS measurements were performed using a Gamry potentiostat. The validity of impedance data was checked using the Kramers–Kronig transform. All measurements were performed with the

Table 2-1. Chemical formula of simulated granitic groundwater for hydrogen induced cracking tests of carbon steel					
Ionic composition, ppm			**Chemical composition, g/L**		
Na^+	1.8×10^3		NaCl	3.8	
Ca^{2+}	4.0×10^2		KCl	0.03	
Mg^{2+}	72		Na_2SO_4	1	
K^+	16		$CaCl_2 \cdot 2H_2O$	1.5	
Cl^-	3.3×10^3		$MgCl_2 \cdot 6H_2O$	0.6	
SO_4^{2-}	6.7×10^2		$NaHCO_3$	0.075	
HCO_3^-	54				

Table 2-2. Solution composition evaluating effects of chloride on Cu corrosion at 50 °C [122 °F]							
Cell	**Solution #**	**Na_2SO_4 (mol/L)**	**$CaCl_2$ (mol/L)**	**NaCl (mol/L)**	**Residual O_2 concentration, ppb**		**Calculated [Cl^-], ppm**
Glass cell set up in glovebox under inert atmosphere	1	0.02*	0	0	0.1–0.2		0
	2	0.02	0.01	0.008	0.1–0.2		1×10^3
	3	0.02	0.01	0.26	0.1–0.2		1×10^4
	4	0.02	0.01	2.8	0.1–0.2		1×10^5
	5	Simulated granitic groundwater			0.1–0.2		3.3×10^3

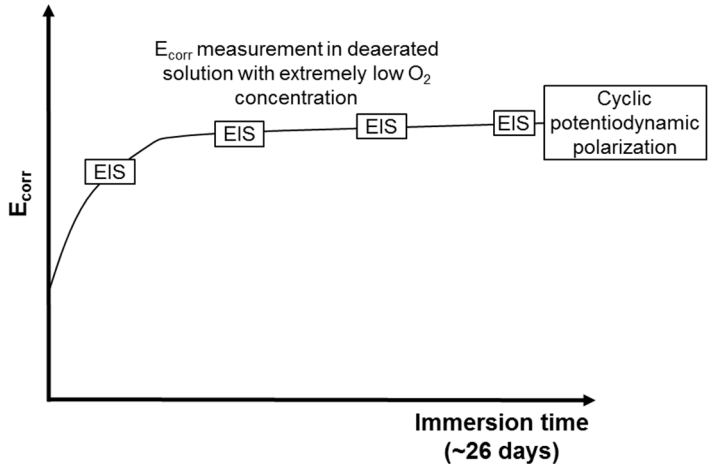

Figure 2-1. Schematics in evaluating effects of chloride on copper corrosion.

potential held at the value of E_{corr} using a perturbation voltage signal of 10 mV applied over the frequency range from 10^{-3} to 10^5 Hz. Ten data points per decade (a factor of 10 in frequency) were recorded. At the end of the tests, a cyclic potentiodynamic polarization scan was performed. The scan started from 100 mV below the E_{corr}, scanning forward up to 800 mV above the E_{corr} and then reversing back to E_{corr}. The scanning rate was 0.167 mV/s during the forward and reverse scans. The total test duration was about 26 days.

2.3 Titanium Corrosion in Brine

2.3.1 Test materials and solution

Three materials were selected to represent Ti materials with different chemical composition and microstructure. Materials used in this test sequence included Ti Grade 2 (commercially pure Ti), Ti Grade 7 (Ti-0.2Pd), and Ti Grade 29 (Ti-6Al-4V-0.1Ru-ELI). Ti Grade 2 was selected as a baseline material for comparison because it does not include any alloying element and is a single α-phase material. Ti Grade 7 was selected because of the addition of palladium (Pd) as a noble element, but it is still a single α-phase material, as is Ti Grade 2. Ti Grade 29 was selected because of the presence of aluminum and vanadium as alloying elements and the addition of ruthenium as a noble element, and because it has both α and β phases. A synthetic brine with composition similar to naturally occurring brines from the reservoirs in the Castile Formation near the Waste Isolation Pilot Plant (WIPP) site was used in the tests of Ti. The chemical formula of this brine is shown in Table 2-3. Chemical reagents including sodium bromide (NaBr), NaCl, KCl, $MgCl_2 \cdot 6H_2O$, $CaCl_2$, Na_2SO_4, and boric acid (H_3BO_3) were used to prepare this solution. The pH before the test was measured to be 4.5±0.2 at ambient temperature and pressure. In a repository in a salt formations, the solution is expected be oxic in the early stages of closure and at elevated temperature. Therefore, most of the tests were conducted at elevated temperature and the test solution was open to the atmosphere.

2.3.2 Electrochemical methods

Table 2-4 lists the electrochemical methods applied to evaluate passivity, localized corrosion, and hydrogen inducing cracking of Ti materials. E_{corr} monitoring and EIS were used to assess passivity and a crevice corrosion test was used to evaluate localized corrosion tendency. The crevice was formed by sandwiching the crevice specimen between polytetrafluoroethylene-tape wrapped ceramic formers, which is the design used in previous work (Dunn et al., 2005). Cyclic potentiodynamic polarization was used to assess repassivation tendency. Cathodic charging was applied to U-bend specimens to assess hydrogen induced cracking under static loading conditions. All of the tests were conducted over the temperature range of 50 to 180 °C [122 to 356 °F]. Glass cells were used for tests conducted below 100 °C [212 °F]. All of the tests above 100 °C [212 °F] were conducted in an autoclave equipped with a high temperature Ag/AgCl reference electrode. Because of schedule constraints, more tests were performed on Ti Grade 7 and limited tests were performed on Ti Grades 2 and 29.

Table 2-3. Chemical formula of brine for corrosion tests of titanium

Ionic composition, mol/kg H_2O			Chemical composition, g/L	
Na^+	6.05		NaBr	1.13
K^+	0.109		NaCl	262
Ca^{2+}	0.0128		KCl	7.23
Mg^{2+}	0.12		$MgCl_2 \cdot 6H_2O$	3.86
Cl^-	5.98		$CaCl_2 \cdot 2H_2O$	1.76
Br^-	0.0124		Na_2SO_4	23.7
SO_4^{2-}	0.191		H_3BO_3	6.0
BO_3^{3-}	0.097			

Table 2-4. Electrochemical methods to assess titanium corrosion					
Aerated solution*			**Deaerated solution†**		
• E_{corr} monitoring and EIS to assess passivity • Crevice corrosion to assess localized corrosion	• Ti Grade 7 • Ti Grade 2		• Cyclic potentiodynamic polarization to assess repassivation	• Ti Grade 7 • Ti Grade 2 • Ti Grade 29	
			• Cathodic charging to assess hydrogen induced cracking	• Ti Grade 7 • Ti Grade 29	
*Solution exposed to atmosphere †Solution bubbled with N_2 gas					

3 EXPERIMENTAL RESULTS AND DISCUSSION

The experimental results are described in this chapter in the same order as the experimental approaches in Section 2.

3.1 Hydrogen Induced Cracking of Carbon Steel under Static Load

The experimental approaches were described in Section 2.1. Cathodic charging tests were conducted at 20 °C [68 °F], 50 °C [122 °F], and 80 °C [176 °F] in N_2-deaerated simulated granitic groundwater. Figure 3-1 shows the cathodic charging current and potential and the U-bend after charging for one test conducted at 20 °C [68 °F]. The cathodic potential was held at −1.2 V_{SCE}, but the charging current decreased with time indicating the increase of resistance. Post-test examination found that the specimen was covered with a layer of white crust, which is likely hydroxides produced from cathodic reaction of H_2O, as indicated in Eq. (3-1). After removing the white deposits, no cracking and no corrosion were observed. The formed hydroxides may have passivated the carbon steel for corrosion and hydrogen entry.

$$H_2O + e^- \rightarrow H + OH^- \quad (3\text{-}1)$$

Figure 3-2 shows the cathodic charging current and potential, and the U-bend after charging for two tests conducted at 50 °C [122 °F]. For the first test with charging duration about 65 days shown in Figure 3-2(a), the cathodic potential was held at −1.2 V_{SCE}, but the charging current decreased with time similar to the trend shown in Figure 3-1. The specimen was covered with a layer of white crust with some corrosion spots. After removing the white deposits, no cracking was observed, but there was light corrosion. In the second test with charging duration of about 90 days shown in Figure 3-2(b), the solution was acidified to pH 2 in an attempt to dissolve the hydroxides and enhance hydrogen entry into the specimen. Furthermore, the U-bend apex exposed to the solution was reduced to about one fifth of the one shown in Figure 3-2(a) to increase the current density. In this test, the working electrode and counter electrode were separated by a salt bridge to avoid solution contamination with products from the anode. The actual potential did not reach the applied potential of −1.2 V_{SCE} and the current was smaller because of the added solution resistance through the salt bridge. After charging, the specimen was covered with a layer of corrosion products, but no cracking was observed.

Figure 3-3 shows the cathodic charging current and potential and the U-bend after charging for two tests conducted at 80 °C [176 °F]. For the first with charging duration of about 31 days shown in Figure 3-3(a), the cathodic potential was held at −1.2 V_{SCE}, but the charging current decreased with time similar to the trends shown in Figures 3-1 and 3-2. The specimen was covered with white crust. After removing the white deposits, no cracking was observed. In the second test with charging duration of about 19 days shown in Figure 3-3(b), the U-bend apex was coated with Microstop™ paint as crevice former in an attempt to establish a localized acidic environment to enhance hydrogen entry into the specimen. The charging potential and current were similar to those in Figure 3-3(a). After charging and removing the paint, crevice corrosion was observed, but no cracking was observed. Previous work (He and Ahn, 2017a) showed that the A516 Grade 60 carbon steel used in this study had high resistance to hydrogen induced cracking under static loading in alkaline water. The additional tests described above indicate that this material also has high resistance to hydrogen induced cracking, even in acidified solution and with a creviced surface over the test duration of 90 days at elevated temperature up to 80 °C [176 °F].

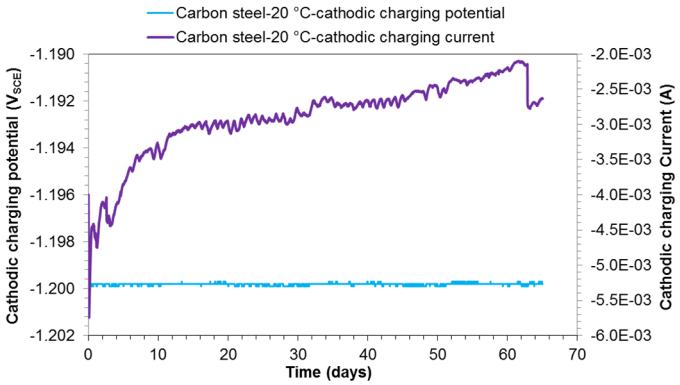

(a)

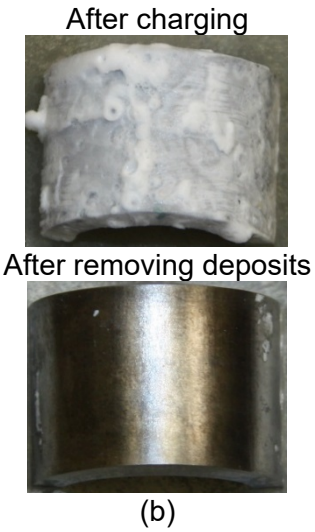

(b)

Figure 3-1. (a) Cathodic charging potential and current of carbon steel in simulated granitic groundwater (pH = 6.65 before test) at 20 °C [68 °F] and (b) post-charging carbon steel U-bend apex.

Kursten and Gaggiano (2018) conducted slow strain rate tests to study the stress corrosion cracking behavior of plain and welded carbon steel exposed to simulated concrete pore water under anoxic conditions at 140 °C [284 °F]. In these tests, the specimens were strained in tension at a constant strain rate of 5×10^{-7} s^{-1} at open circuit potential until they ruptured. Under some conditions, the material fractured, indicating susceptibility to cracking. The main difference is the dynamic loading employed by Kursten and Gaggiano (2018) compared to the static loading used in the current study. The loading condition may have made the significant difference on the observation of cracking resistance.

3.2 Effects of Chloride on Copper Corrosion

The experimental details of this part of the study are described in Section 2.2. Corrosion potential (E_{corr}), electrochemical impedance spectroscopy (EIS), and cyclic potentiodynamic polarization were used to evaluate the effects of chloride on copper (Cu) corrosion. The results are discussed in the following sections.

3.2.1 Corrosion potential (E_{corr})

Figure 3-4(a) shows the E_{corr} of Cu measured prior to each EIS measurement at 50 °C [122 °F]. In each solution, E_{corr} reached relatively steady values in less than 3 days. The E_{corr} values at the end of each test are plotted against logarithmic chloride (Cl^-) concentration in Figure 3-4(b). As was observed in previous work (He and Ahn, 2018), E_{corr} decreased almost linearly with the logarithm of the Cl^- concentration. This relationship suggests that the corrosion process may be controlled by mass transport.

3.2.2 Potentiodynamic polarization

Figure 3-5(a) shows the results of cyclic potentiodynamic polarization experiments in the 5 solutions with O_2 concentrations of about 0.1–0.2 ppb at 50 °C [122 °F]. The curves associate with forward and backward scans are plotted separately in Figures 3-5(b,c) for clarity. Above the potential at net zero current, the current increased with anodic polarization indicating anodic

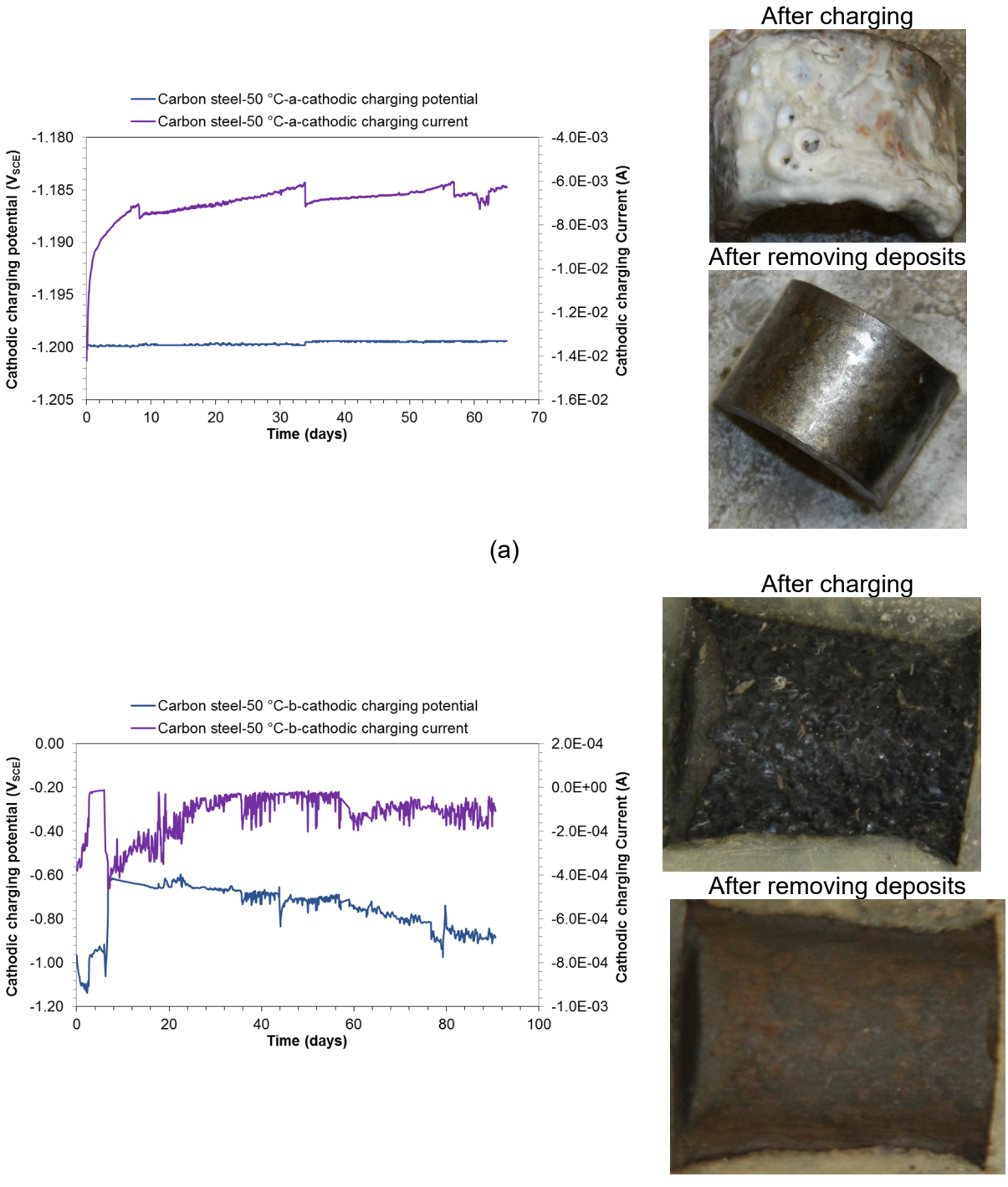

Figure 3-2. Cathodic charging potential and current at 50 °C [122 °F] and post-charging carbon steel specimens in (a) simulated granitic groundwater (pH = 6.65 before test) and (b) acidified simulated granitic groundwater (pH = 2 before test).

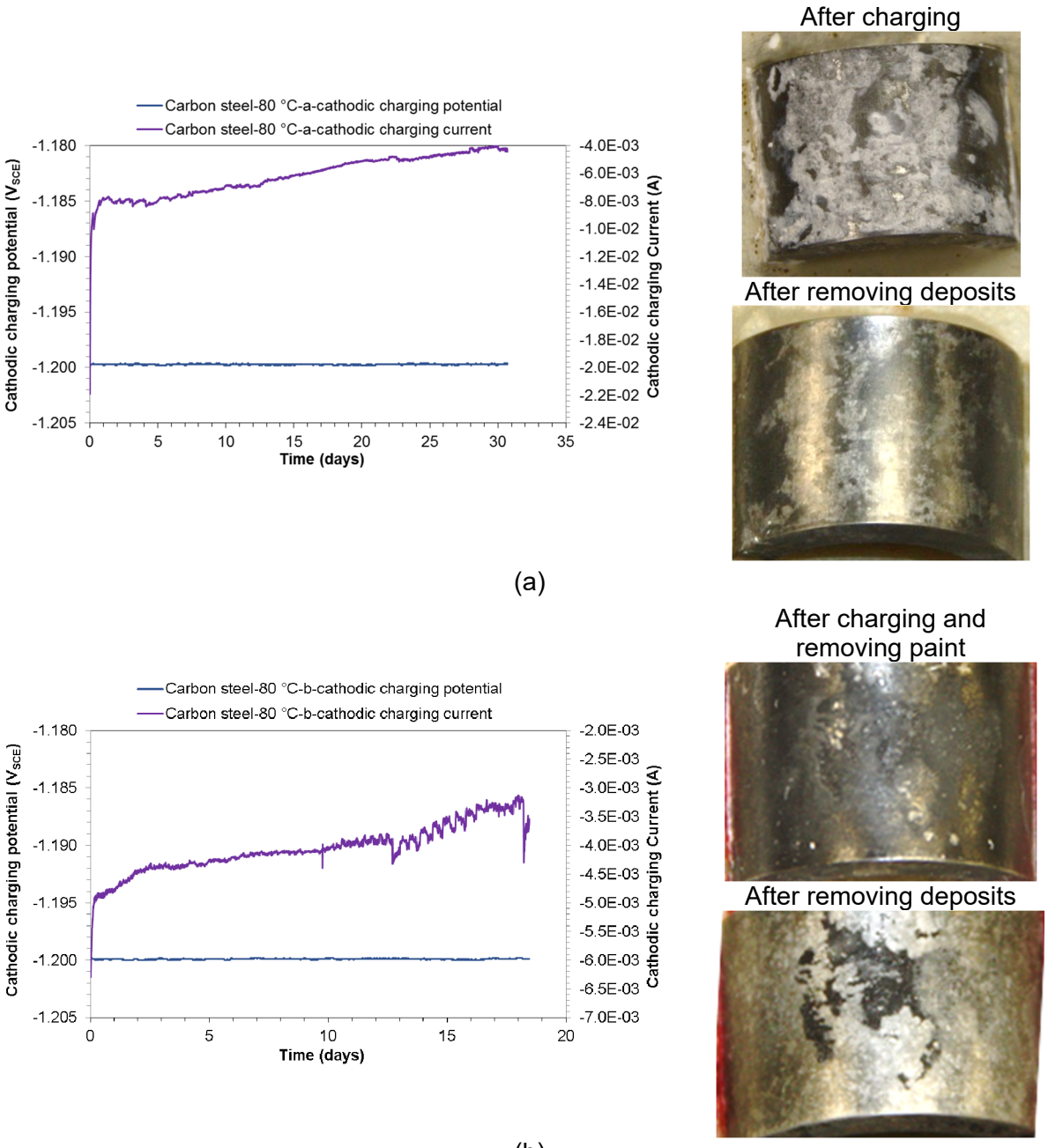

Figure 3-3. Cathodic charging potential and current in simulated granitic groundwater (pH = 6.65 before test) at 80 °C and post-charging carbon steel specimens (a) U-bend apex was exposed to solution and (b) U-bend apex was covered with Microstop™ paint as crevice former.

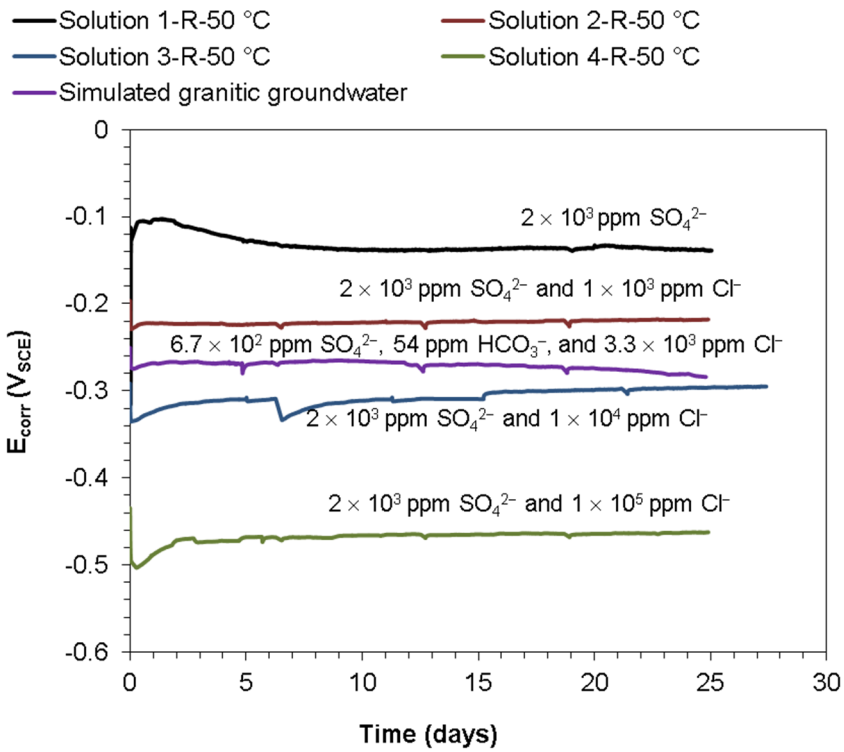

(a)

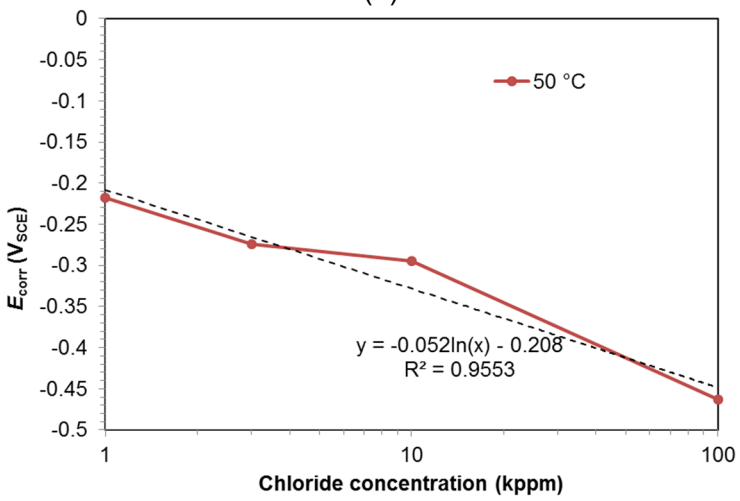

(b)

Figure 3-4. **(a) E_{corr} of Cu as a function of time in five solutions with varying Cl^- concentration at 50 °C [122 °F], and (b) relatively steady E_{corr} at the end of each test as a function of Cl^- concentration.**

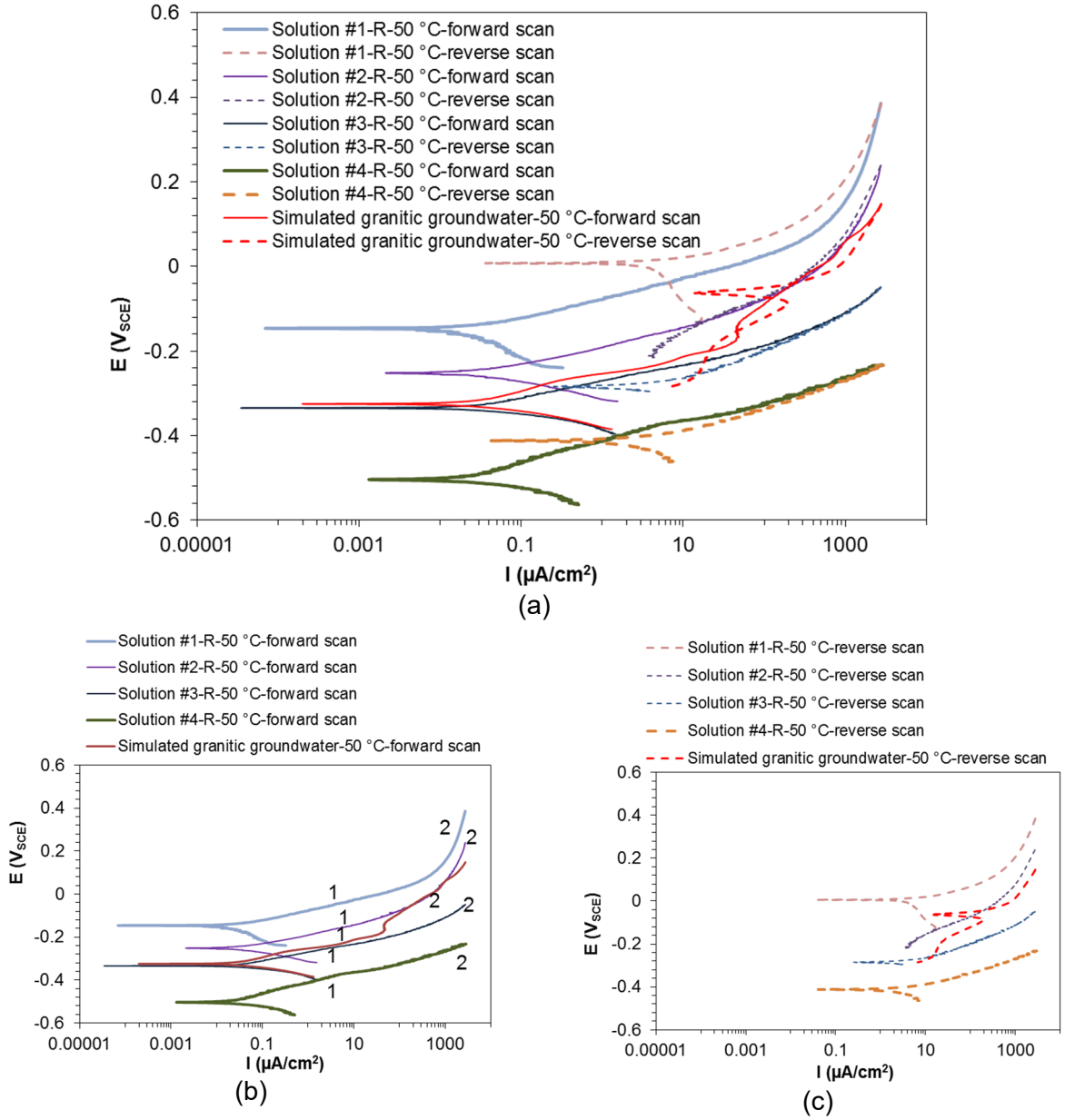

Figure 3-5. Cyclic voltammograms on copper in five solutions at 50 °C [122 °F] (a) forward and backward scans, (b) forward scan , and (c) backward scan. Solution 1: 2×10^3 ppm SO_4^{2-}; Solution 2: 2×10^3 ppm SO_4^{2-} and 1×10^3 ppm Cl^-; Solution 3: 2×10^3 ppm SO_4^{2-} and 1×10^4 ppm Cl^-; Solution 4: 2×10^3 ppm SO_4^{2-} and 1×10^5 ppm Cl^-; Solution 5: simulated granitic groundwater.

dissolution. For the solutions containing Cl^-, two anodic peaks on the forward scan were observed. The numbers (1 and 2) in Figure 3-5(b) indicate the two stages of current change with potential separated by the first anodic peak. The different stages could be associated with changes of charge transfer and mass transport controlling kinetics and the formation of different corrosion product layers on the surface, as observed by Kear et al. (2004). On the reverse scan the current decreased with time, then switched to a cathodic reaction. The potential at net zero current shown on the reverse scan was higher than on the forward scan, which could indicate surface modification by corrosion products. During both forward and reverse scans, potential

at net zero current consistently decreased and current density increased with increasing Cl^- concentration. The anodic polarization data during the forward scan show two Tafel regions, as indicated by the numbers (1 and 2) in Figure 3-5(b). They are fitted with the Tafel relationship shown in Eq. (3-2).

$$\eta = k \ln\left(\frac{i}{i_0}\right) \tag{3-2}$$

where η is the overpotential, k is the Tafel slope, i is the current density, and i_0 is the exchange current density. The Tafel regions and the fitting lines are shown in Figure 3-6. The Tafel slopes and i_0 from these 5 solutions are summarized in Table 3-1. In both regions, i_0 increased significantly with increasing Cl^- concentration, indicating higher corrosion rates at higher Cl^- concentration.

3.2.3 Electrochemical Impedance Spectroscopy

Figures 3-7 through 3-11 show the EIS data obtained at various times from tests involving four solutions with varying Cl^- concentration and simulated granitic groundwater at 50 °C [122 °F]. The figures include curves computed from equivalent circuits approximating the electrochemical system. The data show a mix of resistive and capacitive behavior. One distinctive feature is that all the EIS spectra were different in each of the five solutions.

The principal observations from each set of data are as follows.

- The EIS data from Solution 1 containing SO_4^{2-} showed two time constants (τ) marked with numbers (1 and 2) in the Nyquist plot and phase angle plot in Figure 3-7. An equivalent electric circuit in Figure 3-12(a) was used to model the EIS data. This circuit consists of solution resistance (R_s), polarization resistance (R_p), film resistance (R_f), constant phase element of double layer (CPE_{dl}), and constant phase element of film (CPE_f). The physical model associated with this circuit represents a film on the metal surface, with some discontinuities or fractures where efficient electron transfer may occur. The chemical composition of this film is unknown; the film may be a thin layer of corrosion products. The data were well reproduced with a two-τ circuit. The fitting results are summarized in Table 3-2. R_p varied by more than one order of mangitude, with high fitting uncertainty. The corrosion rate was calculated from R_p based on Eq. (3-3). The computed R_p corresponds to a corrosion rate in the range of several to tens of nanometers per year. The corrosion rates are also included in Table 3-2.

$$Corrosion\ rate = \frac{k\ B\ EW}{R_p\ \rho} \tag{3-3}$$

where

k = constant
B = Stern-Geary Constant (0.027 V assumed)
R_p = polarization resistance
ρ = density {8.94 g/cm^3 [0.322 lb/in^3] for copper}
EW = material equivalent weight {63.5 g [2.22 oz] for copper}

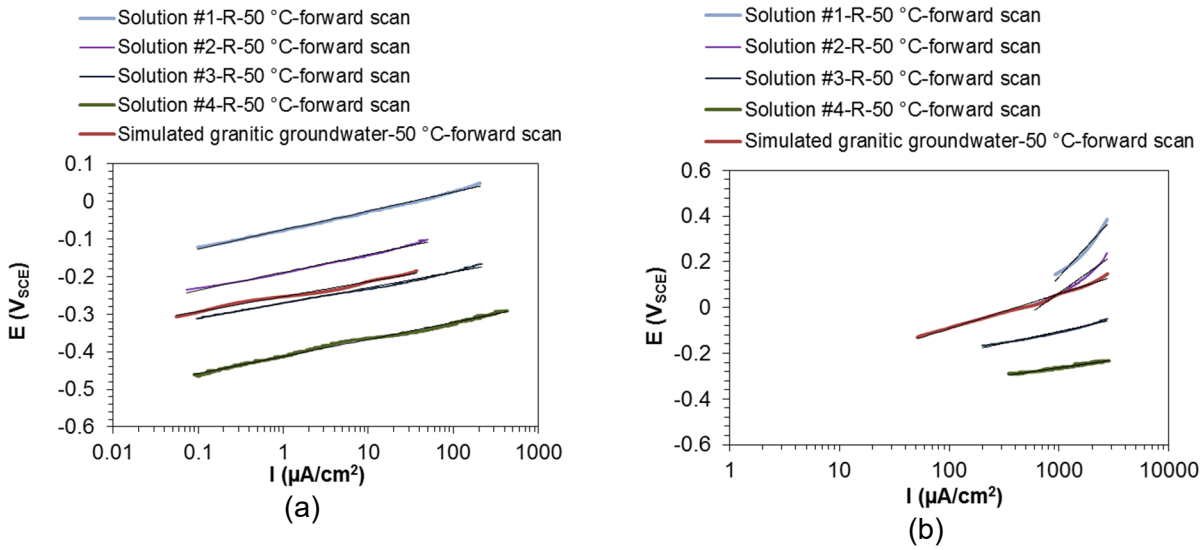

Figure 3-6. **Tafel regions and the fit to Tafel equation for the data in forward scan (a) region 1 and (b) region 2 in Figure 3-4(b). Solution 1: 2×10^3 ppm SO_4^{2-}; Solution 2: 2×10^3 ppm SO_4^{2-} and 2×10^3 ppm Cl^-; Solution 3: 2×10^3 ppm SO_4^{2-} and 2×10^4 ppm Cl^-; Solution 4: 2×10^3 ppm SO_4^{2-} and 2×10^5 ppm Cl^-.**

Table 3-1. Tafel slopes and exchange current density for anodic polarization of Cu at 50 °C [122 °F]

Tafel regions	Fitting parameters	Solution 1 (2×10^3 ppm SO_4^{2-})	Solution 2 (2×10^3 ppm SO_4^{2-} and 1×10^3 ppm Cl^-)	Simulated granitic groundwater	Solution 3 (2×10^3 ppm SO_4^{2-} and 1×10^4 ppm Cl^-)	Solution 4 (2×10^3 ppm SO_4^{2-} and 1×10^5 ppm Cl^-)
Region 1	Tafel slope, mV	22	20	17	18	21
	i_0, μA/cm²	32	1.3×10^4	3.0×10^6	3.4×10^6	3.5×10^8
Region 2	Tafel slope, mV	228	147	66	45	30
	i_0, μA/cm²	553	650	403	1.0×10^4	7.7×10^6

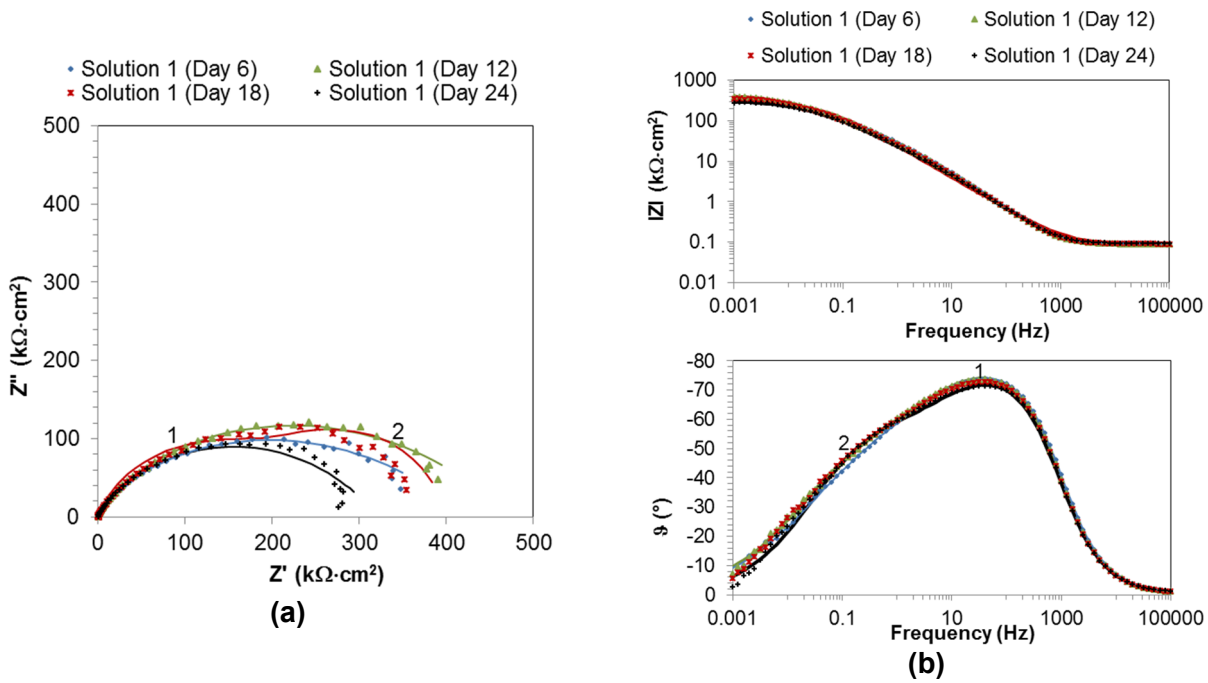

Figure 3-7. **EIS of Cu exposed to Solution 1 at 50 °C [122 °F] (2×10^3 ppm SO_4^{2-}) at 6, 12, 18, and 24 days; (a) Nyquist plot and (b) Bode plot. The numbers (1 and 2) in the plots indicate inflections associated with different time constants.**

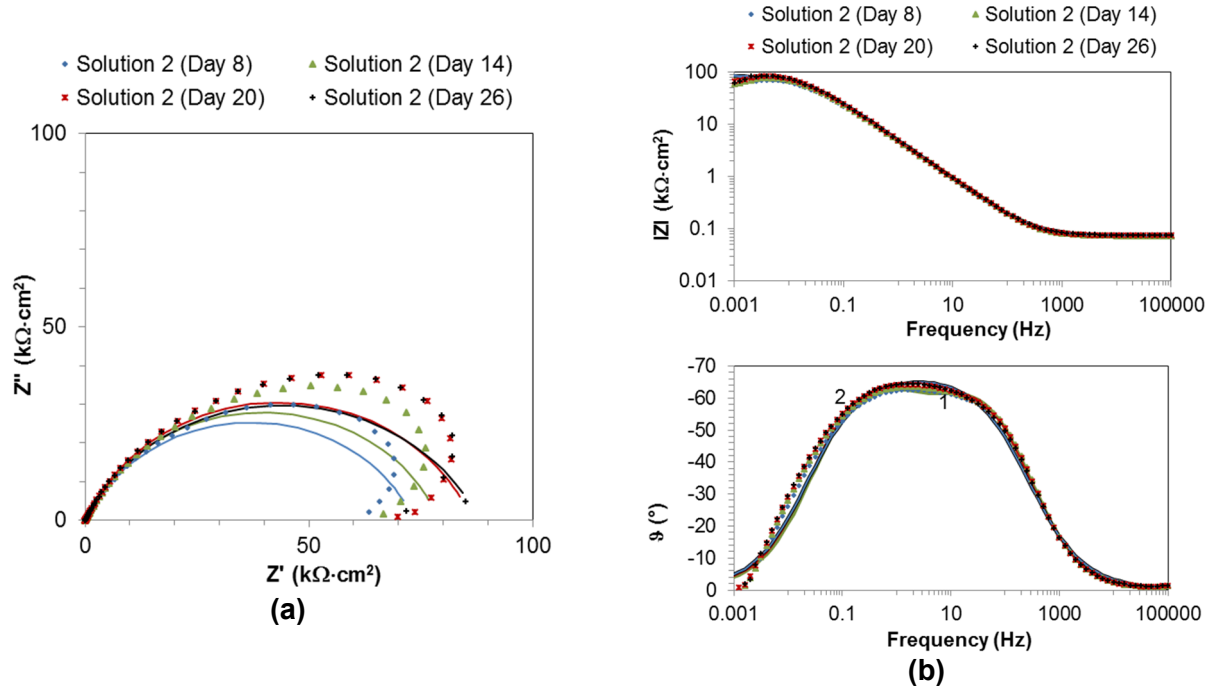

Figure 3-8. **EIS of Cu exposed to Solution 2 (2×10^3 ppm SO_4^{2-} and 1×10^3 ppm Cl^-) at 50 °C [122 °F] at 8, 14, 20, and 26 days; (a) Nyquist plot and (b) Bode plot. The numbers (1 and 2) in the plots indicate inflections associated with different time constants.**

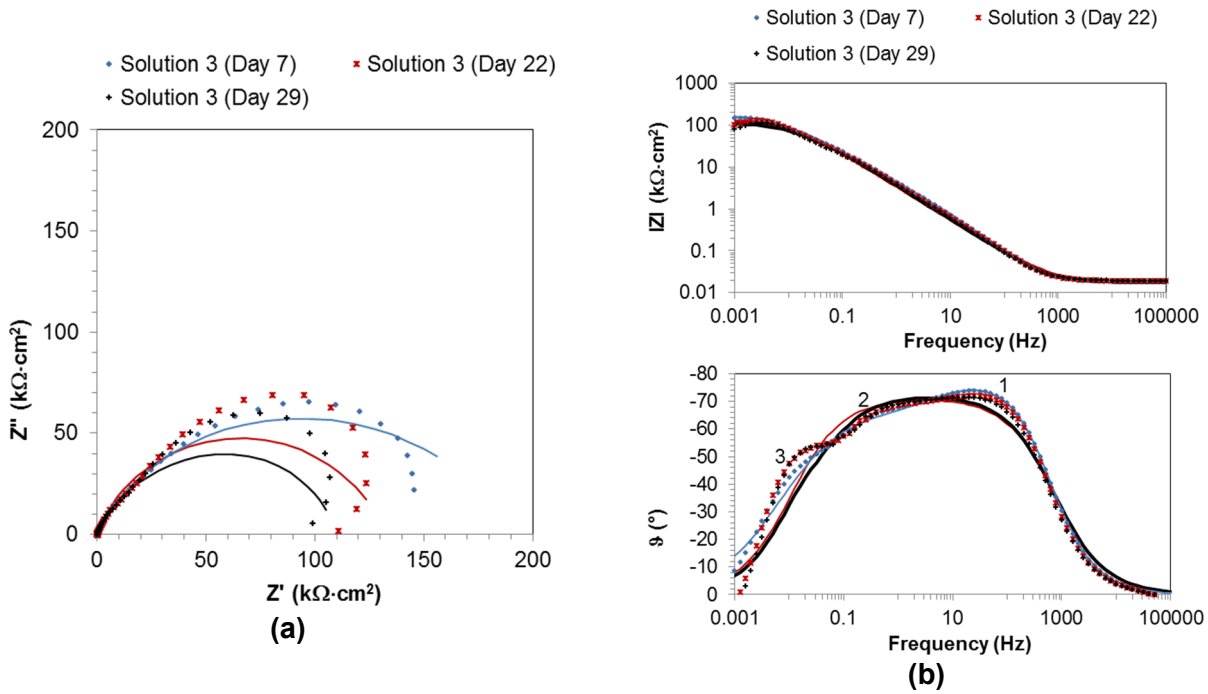

Figure 3-9. EIS of Cu exposed to Solution 3 (2×10^3 ppm SO_4^{2-} and 1×10^4 ppm Cl^-) at 50 °C [122 °F] at 7, 22, and 29 days; (a) Nyquist plot and (b) Bode plot. The numbers (1, 2, and 3) in the plots indicate inflections associated with different time constants.

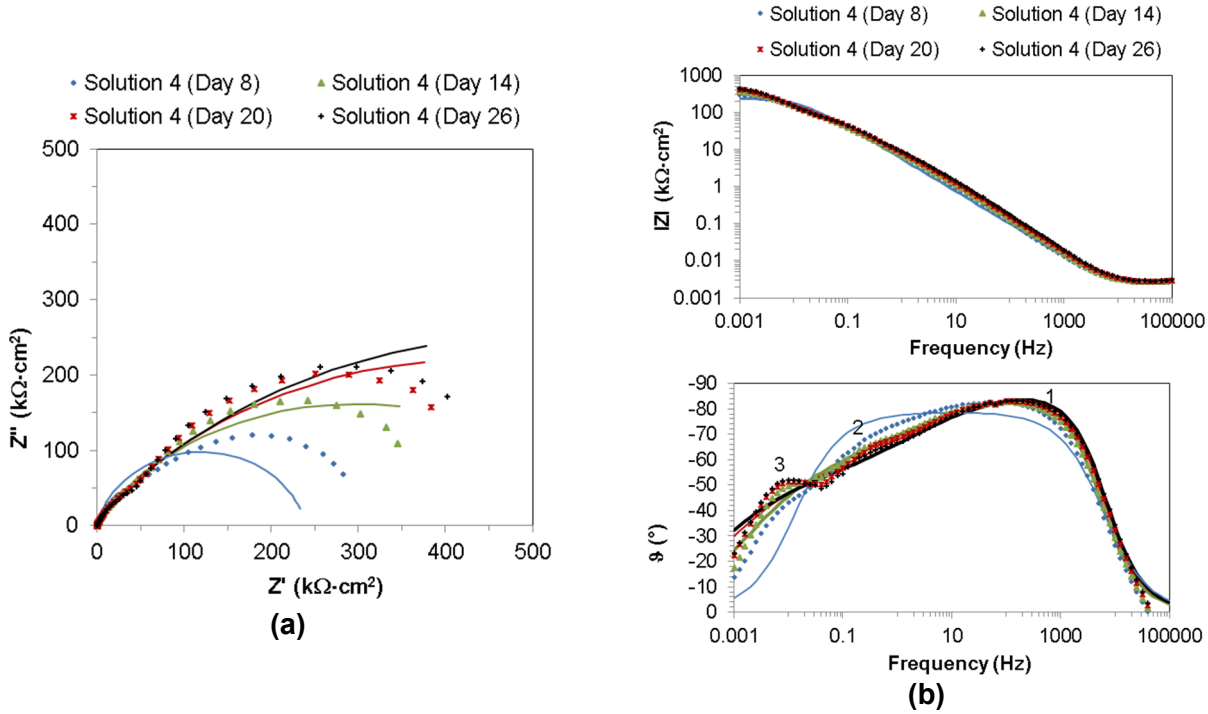

Figure 3-10. EIS of Cu exposed to Solution 4 (2×10^3 ppm SO_4^{2-} and 1×10^5 ppm Cl^-) at 50 °C [122 °F] at 8, 14, 20, and 26 days at 50 °C [122 °F]; (a) Nyquist plot and (b) Bode plot. The numbers (1, 2, and 3) in the plots indicate inflections associated with different time constants.

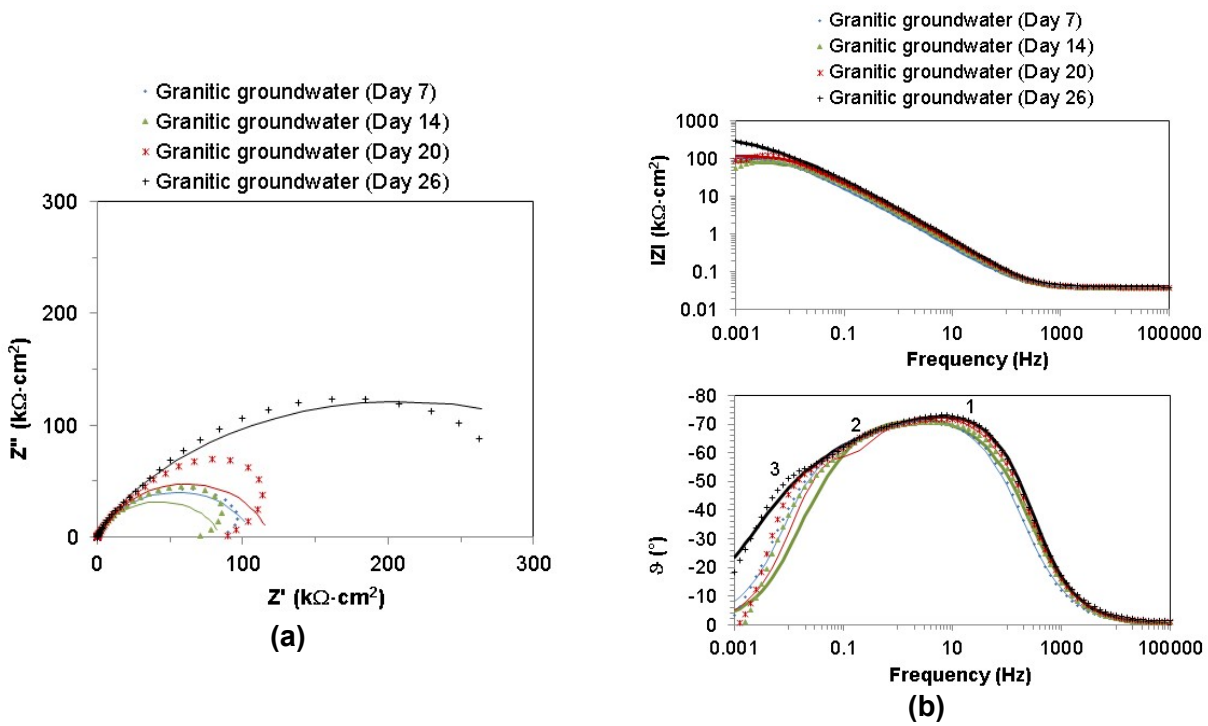

Figure 3-11. EIS of Cu exposed to simulated granitic groundwater at 50 °C [122 °F] at 7, 14, 20, and 26 days at 50 °C [122 °F]; (a) Nyquist plot and (b) Bode plot. The numbers (1, 2, and 3) in the plots indicate inflections associated with different time constants.

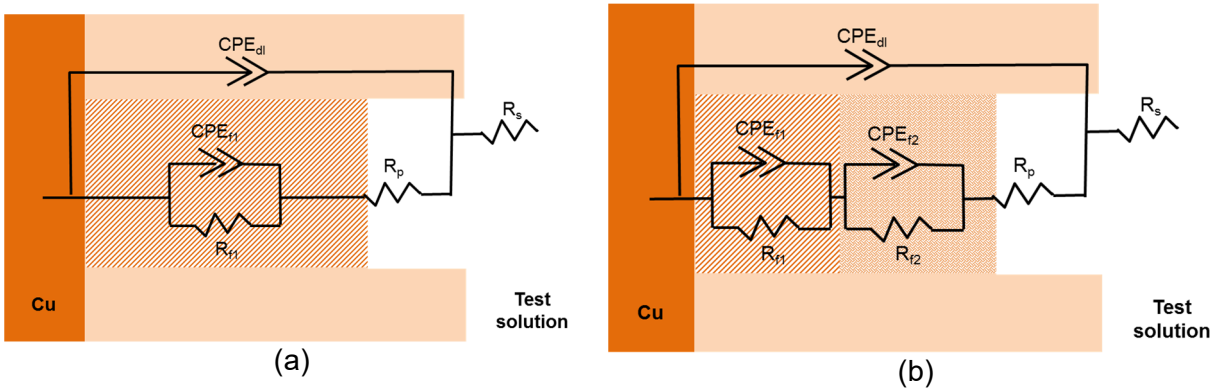

Figure 3-12. (a) Two- and (b) three-time constant circuits used to model the EIS data in Figures 3-7 through 3-11. R_s: solution resistance; R_p: polarization resistance; R_f: film resistance; CPE_{dl}: constant phase element of double layer; CPE_f: constant phase element of film.

Table 3-2. Corrosion parameters and Cu corrosion rates at 50 °C [122 °F] derived by fitting equivalent circuits to the EIS data						
Solution #	**Time (days)**	**R_p ($k\Omega \cdot cm^2$)**	**R_{film} ($k\Omega \cdot cm^2$)**	**C_{dl} ($\mu F \cdot cm^2$)**	**R_s (Ω)**	**Corrosion rate calculated from R_p (nm/y)**
1 (2×10^3 ppm SO_4^{2-})	6	16.8	406	4	9.7	37.3
	12	19.2	452	5	9.7	32.6
	18	266	134	10	9.4	2.4
	24	14.2	307	5	10.1	44.3
2 (2×10^3 ppm SO_4^{2-} and 1×10^3 ppm Cl^-)	8	3.7	69.7	33	8.1	169
	14	4.7	74.3	34	7.9	134
	20	4.7	81.7	34	8.0	134
	26	83.5	18.0	49	8.0	8
3 (2×10^3 ppm SO_4^{2-} and 1×10^4 ppm Cl^-)	7	—*	190	32	2.0	—*
	22	—*	132	65	1.9	—*
	29	—*	25	63	1.9	—*
4 (2×10^3 ppm SO_4^{2-} and 1×10^5 ppm Cl^-)	8	0.02	240	35	0.29	—*
	14	0.36	611	11	0.30	1,756
	20	0.26	899	10	0.31	2,402
	26	0.26	1,060	8	0.31	2,445
Simulated granitic groundwater	7	32	75	74	4.1	20
	14	76	9	65	4.0	8
	20	42	76	49	4.2	15
	26	1	435	26	4.3	1,000
*High fitting uncertainty makes ambiguous the value of R_p						

- The EIS data from Solution 2 containing 2×10^3 ppm SO_4^{2-} and 1×10^3 ppm Cl^- also showed two τ values, identified by the labeled inflections in the phase angle plot in Figure 3-8(b). The results from fitting the two-τ circuit are included in Table 3-2. On average, the film resistance and R_p were lower than those from Solution 1, consistent with the notion that the addition of Cl^- increases corrosion rates.

  The EIS data from Solution 3 containing 2×10^3 ppm SO_4^{2-} and 1×10^4 ppm Cl^- showed two τ values from one measurement and three τ values in the remaining measurements. The τ values are marked in the phase angle plot in Figure 3-9(b). Changes in τ suggest changes in film structure due to exposure to different solutions. A three-τ circuit representing two different layers of film inside the discontinuities in parallel with the double layer capacitance shown in Figure 3-12(b) fits the data well, but the fitting uncertainty (i.e., the error in fitting the data to the model) was high. Only the parameters with low fitting uncertainty are included in Table 3-2. Because of the high fitting uncertainty of R_p, the corrosion rates based on R_p estimates were not calculated.

- The EIS data from Solution 4 containing 2×10^3 ppm SO_4^{2-} and 1×10^5 ppm Cl^- also suggests three τ values, but corresponding peaks and inflections in the phase diagram are not clearly exhibited. Inflections and peaks suggesting different □ values are marked in the phase angle plot in Figure 3-10(b). The data cannot be approximated well with either of the circuits in Figure 3-12, especially for the first set of data. To keep the model simple, the results from fitting the two-τ equivalent circuit in Figure 3-12(a) are summarized in Table 3-2. On average, the polarization resistance was lower than resistances associated with Solution 1, consistent with the notion that the addition of Cl^- increases corrosion rates.
- The EIS data from the simulated granitic groundwater suggest nearly three τ values, but the peaks in the phase diagram are not clearly exhibited. The inflections suggesting different τ values are marked in the phase angle plot in Figure 3-12(b). The data can be approximated well with either of the circuits in Figure 3-12. To keep the model simple, the results from fitting the two-τ circuit in Figure 3-12(a) are summarized in Table 3-2. On average, the polarization resistances were lower than those from Solution 1.

The averaged polarization resistance, corrosion rate, double layer capacitance, and solution resistance of Cu exposed to the five solutions at 50 °C [122 °F] derived by fitting circuits (Figure 3-12) to the EIS data (Figures 3-7 through 3-11) are plotted in Figure 3-13. R_p was the lowest for the solution with the highest Cl^- concentration at 50 °C [122 °F], and except for the dip for Solution 2, R_p decreased with increasing Cl^- concentration, indicating increasing corrosion rates with increasing Cl^-. C_{dl} increased, then decreased with the Cl^- concentration, which could be due to the film structure changes. The solution resistance decreased with increasing Cl^- concentration.

3.2.4 Discussion

Literature information demonstrates that Cl^- plays a significant role in corrosion of Cu, especially in oxic solutions, because Cu(I) complexation forms cuprous-chloro complex ions supported by O_2 or other cathodic reactants such as Cu^{2+} (Kear et al., 2004). The possible anodic reactions in an oxic Cl^--containing solution are:

$$Cu + Cl^- \rightarrow CuCl_{ads} + e^- \quad (3\text{-}4)$$

$$CuCl_{ads} + Cl^- \rightarrow CuCl_2^- \quad (3\text{-}5)$$

These anodic reactions are generally fast and the rates are limited by the transport of dissolved Cu(I) away from the interface. Example cathodic reactions (Betova et al., 2013) in an oxic Cl^--containing solution are:

$$O_2 + 2H_2O + 4e^- \rightarrow 4OH^- \quad (3\text{-}6)$$

$$Cu^{2+} + 2Cl^- + e^- \rightarrow CuCl_2^- \quad (3\text{-}7)$$

The cathodic reactions are probably under both electron transfer and mass transport control. When exposed to oxic environments, Cu typically forms a duplex corrosion product layer, such as an underlying layer of Cu_2O covered by $CuCl_2 \cdot 3Cu(OH)_2$, or other structures depending on the environment (Kear et al., 2004). However, in anoxic chloride-containing solutions, some studies show no evidence for Cu corrosion (Simpson and Schenk, 1987; Eriksen et al., 1989; Hedin et al., 2018). Research sponsored by SKB (Hedin et al., 2018) showed that the following

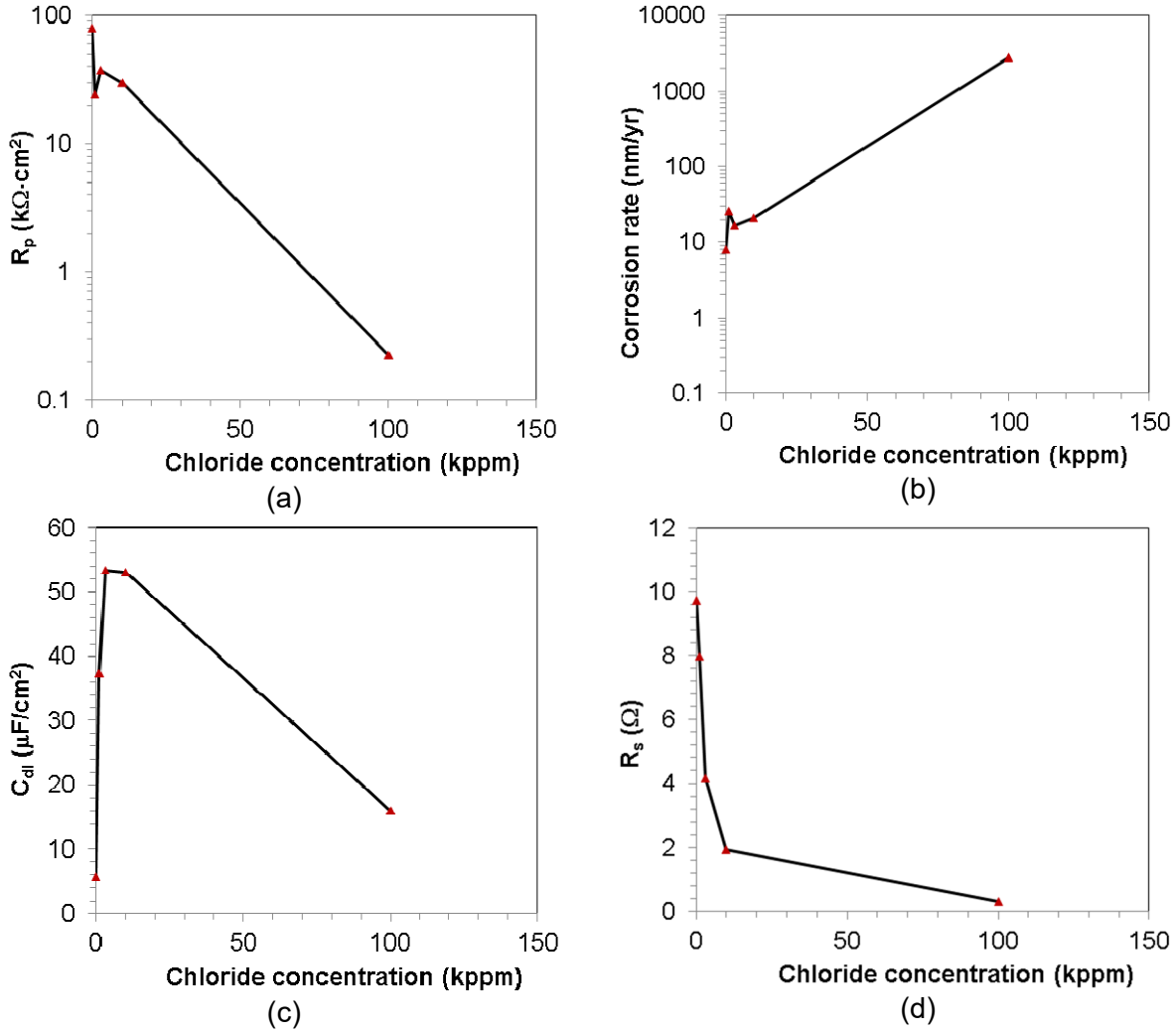

Figure 3-13. Averaged (a) polarization resistance, (b) corrosion rate, (c) double layer capacitance, and (d) solution resistance of Cu exposed to five solutions at 50 °C [122 °F] derived by fitting the equivalent-circuit model in Figure 3-12(a) to the EIS data in Figures 3-7 through 3-11.

cathodic reaction producing H_2 is not a feasible path to support Cu corrosion in anaerobic neutral solutions:

$$2H_2O + 2e^- \rightarrow H_2 + 4OH^- \quad (3\text{-}8)$$

Figures 3-4 and 3-5 and Tables 3-1 and 3-2 show that E_{corr} decreased, anodic current density increased, Tafel slope decreased, exchange current density increased, and corrosion rate increased with increasing Cl^- concentration. All these results consistently demonstrate that Cl^- played a consistent role in enhancing corrosion of copper in solutions with O_2 concentrations of 0.1–0.2 ppb. The results also corroborate the observation from previous work conducted under the same conditions in FY 2018 (He and Ahn, 2018). Figure 3-14 illustrates schematically the Tafel approximation for the polarization curves for both the cathodic and anodic reactions. Higher Cl^- concentration could have depolarized the anodic reaction, resulting in lower E_{corr} values and potentially larger i_{corr}.

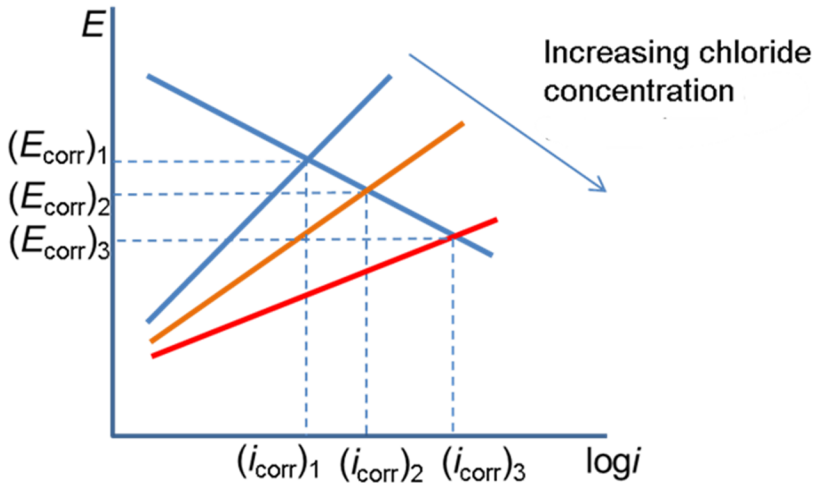

Figure 3-14. Effect of increasing Cl^- concentration on the E_{corr} and corrosion tendency.

The several time constants indicated by the numbers (1, 2, and 3) in the EIS data in Figures 3-8(b) through 3-11(b) suggest a layered film structure formed on the metal surface. This could indicate the formation of Cu_2O or $CuCl_2 \cdot 3Cu(OH)_2$, commonly observed in oxic solutions. However, the observations of corrosion products and non-negligible corrosion rates seem to be in conflict with information in the literature reporting lack of Cu corrosion in anoxic solutions. The nature of the cathodic reaction in this work is uncertain. There are several possibilities for cathodic reactions: (i) reduction of trace amounts of O_2 in solution, (ii) reduction of Cu^{2+} in the air-formed oxide, (iii) reduction of H_2O to H_2, and (iv) reduction of trace amount of heavy-metal contaminants. At high Cl^- concentration, the kinetic rate is high (indicated by the large exchange current density) and the controlling factor could be mass transport of cathodic reactants. To reconcile the results of this study with information in the literature, further work is needed to evaluate the cathodic reactions, the film, and the corrosion products using more sensitive analytical methods over longer times.

3.3 Titanium Corrosion in Brine

The experimental details are described in Section 2.3. Ti Grades 2, 7, and 29 were included in the study, but most of the work was on Ti Grade 7, followed by Ti Grades 2 and 29. The results are presented in the following sections in the order from Ti Grades 7, 2, and then 29.

3.3.1 Titanium Grade 7

3.3.1.1 Corrosion potential in aerated brine

Three tests were conducted under aerated conditions to measure E_{corr}: (i) Test 1 at 80 °C [176 °F]; (ii) Test 2 started at 120 °C [248 °F], then increased temperature to 150 °C [302 °F]; and (iii) Test 3 started at 100 °C [212 °F], then increased temperature sequentially to 120 °C [248 °F], 140 °C [284 °F], 160 °C [320 °F], and 180 °C [356 °F] in weekly increments. The corrosion potential measured under aerated conditions from these three tests is shown in Figure 3-15(a). At each of these temperatures, E_{corr} increased with increasing temperature and time after the initial dip right after exposing the material to the brine. This suggests that the material remains passive over the temperature ranges and the test duration. The E_{corr} in Figure 3-15(a) was in the range of 0.2–0.5 V_{SCE}. Figure 3-15(b) shows the cylindrical electrode

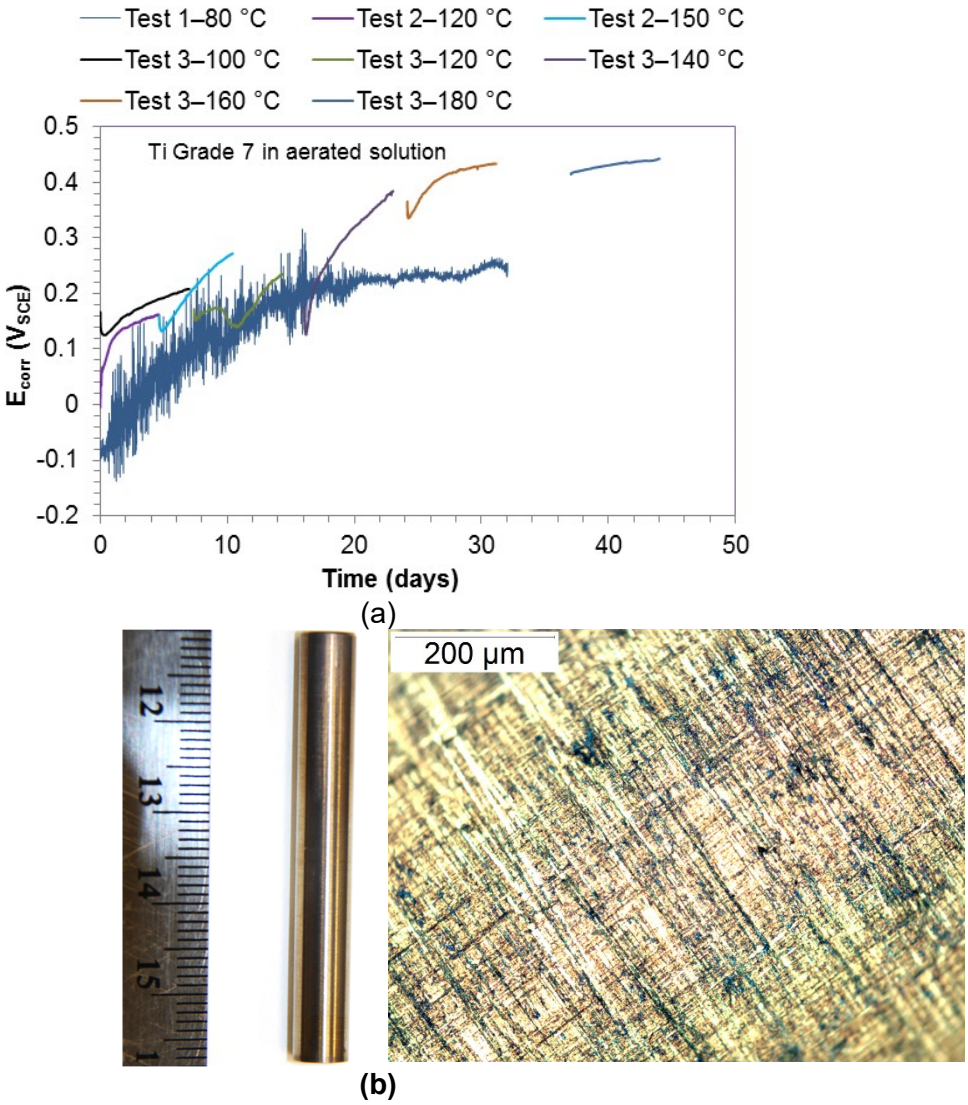

Figure 3-15. (a) E_{corr} of Ti Grade 7 as a function of time at temperatures of 80 °C [176 °F], 100 °C [212 °F], 120 °C [248 °F], 140 °C [284 °F], 160 °C [320 °F], and 180 °C [356 °F] and (b) cylindrical electrode and surface examined under microscope after testing from 100 °C [212 °F] to 180 °C [356 °F] for about 45 days.

after testing from 100 °C [212 °F] to 180 °C [356 °F] for about 45 days. The electrode was examined under the microscope. One photo taken under the microscope is included as the far right picture with a 200 µm scale bar in Figure 3-15(b) as an example to show the passive surface. No pitting was observed.

3.3.1.2 Electrochemical impedance spectroscopy in aerated brine

During the measurement of E_{corr}, EIS was performed about weekly. The EIS results are shown in Figure 3-16. Figures 3-16(a,b) show that the EIS data were highly consistent over the test duration of 30 days, suggesting high stability of the passive film. Two time constants were observed, particularly for the EIS data at 80 °C [176 °F]. The data in the lower frequency region were fit to the commonly used one-time constant circuit (Randles circuit) in Figure 3-17 to obtain

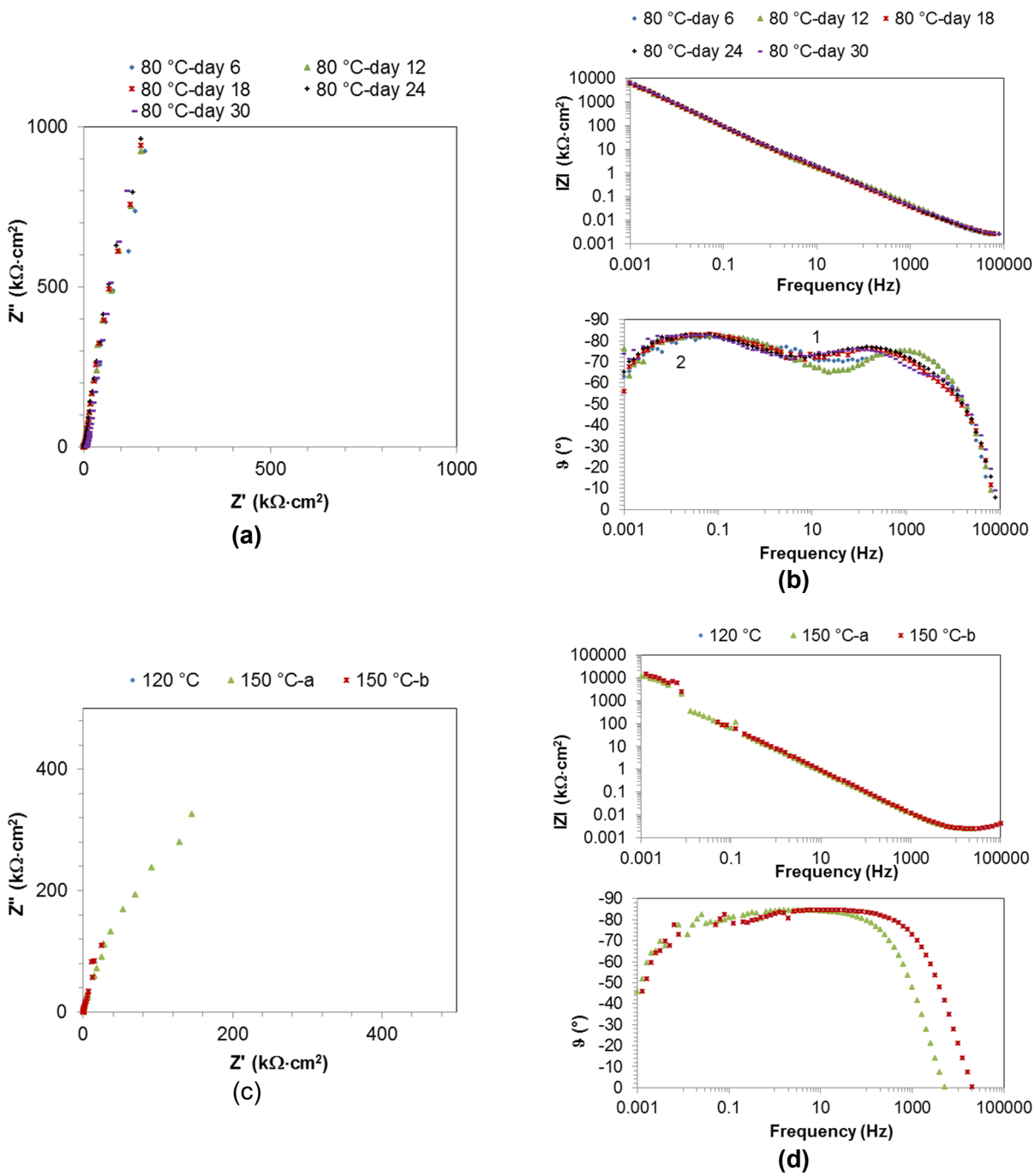

Figure 3-16. EIS of Ti Grade 7 exposed to brine (a) Nyquist plot and (b) Bode plot at 80 °C [176 °F] at 6, 12, 18, 24, and 30 days, (c) Nyquist plot, and (d) Bode plot at 120 °C [248 °F] and 150 °C [302 °F]. The numbers (1 and 2) in the plots label inflections associated with different time constants.

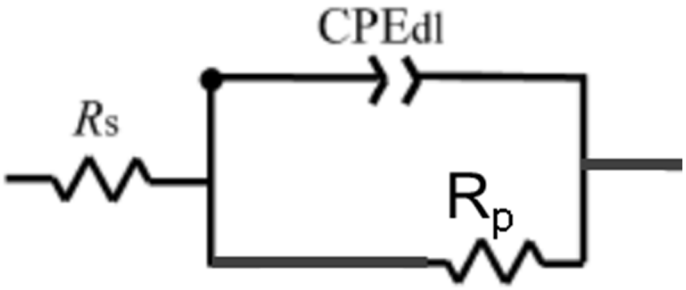

Figure 3-17. Randles circuit used to fit to the EIS data in low frequency region in Figure 3-16. CPE_{dl}: constant phase element of double layer; R_p; polarization resistance; R_s—solution resistance.

R_p and calculate corrosion rates. Corrosion rates were calculated based on equivalent weight of 12 g and density of 4.54 g/cm^3 for titanium. Table 3-3 summarizes the corrosion parameters and corrosion rates of Ti Grade 7 derived by fitting EIS data to the Randles circuit. The computed corrosion rates were less than 1 nanometer per year.

3.3.1.3 Crevice corrosion in aerated brine

Crevice corrosion tests of Ti Grade 7 were performed at 80 °C [176 °F] and 140 °C [284 °F] in brine. During the test, the creviced electrode was coupled to a large Ti Grade 7 plate and the crevice corrosion current and potential were measured. Figure 3-18 shows the current and potential. For the test at 80 °C [176 °F], the potential increased with time in a similar trend as the noncreviced Ti Grade 7 shown in Figure 3-15a, and the current fluctuated at around 0.1 μA without any indication of stable current increase associated with crevice corrosion initiation. The test was terminated at about 40 days. Posttest examination of the specimen showed no indication of crevice corrosion initiation.

For the test at 140 °C [284 °F], the potential increased with time at the beginning, then it stabilized at around 0.35 V_{SCE}. The current stabilized at about 50 μA without any indication of stable current increase associated with crevice corrosion initiation. The test was terminated at about 25 days. Photos of the posttest specimen are shown in Figure 3-18(b). The one at the bottom with a 500 μm scale bar was taken under microscope. The surface was slightly stained, but there was no crevice corrosion initiation.

3.3.1.4 Cyclic potentiodynamic polarization in N_2 deaerated brine

The objective of performing cyclic potentiodynamic polarization was to evaluate the repassivation tendency of Ti Grade 7 in brine. Figure 3-19 shows the cyclic potentiodynamic polarization of Ti Grade 7 in N_2 deaerated brine at 80 °C [176 °F], 95 °C [203 °F], 120 °C [248 °F], 140 °C [284 °F], 160 °C [320 °F], and 180 °C [356 °F], plotted individually for clarity, and including the forward scans and reverse scans in the same plot for comparison. The crevice coupons after polarization are shown in Figure 3-20.

Table 3-3. Corrosion parameters and corrosion rates of Ti Grade 7 derived by fitting EIS to Randles circuit					
Temperature	**Time (days)**	**R_p (MΩ·cm^2)**	**C_{dl} (μF·cm^2)**	**R_s (Ω)**	**Corrosion rate calculated from R_p (nm/y)**
80 °C	6	39	15	0.3	0.0059
	18	47	15	0.3	0.0050
	24	148	14	0.3	0.0016
120 °C	6	21	5	0.5	0.0111
150 °C	6	12	16	0.3	0.0201
	10	15	11	0.3	0.0156

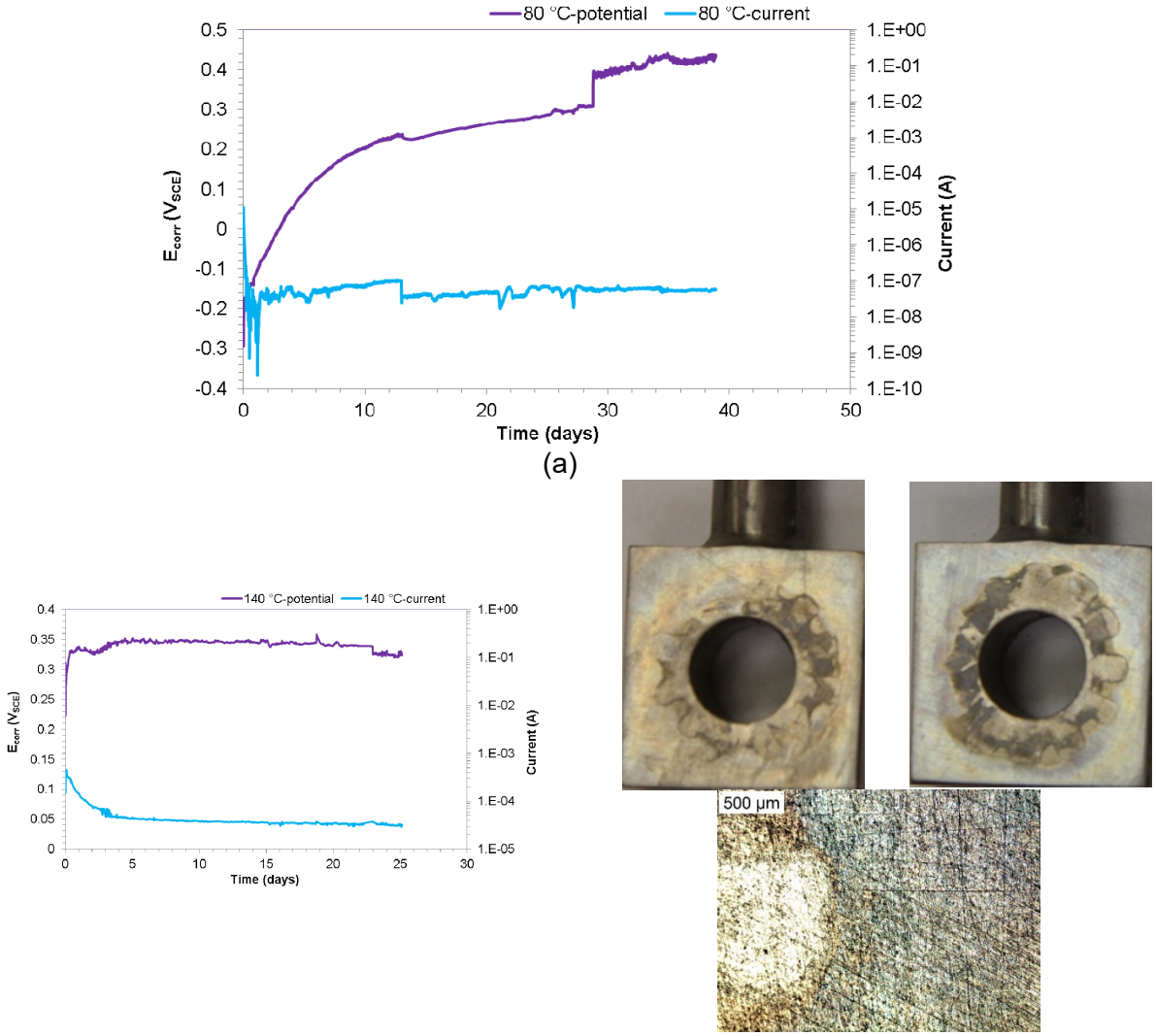

Figure 3-18. Crevice corrosion current and potential of Ti Grade 7 at (a) 80 °C [176 °F] and (b) 140 °C [284 °F] in brine. Figure (b) also shows posttest photos of the 140 °C [284 °F] specimen. The picture at the bottom was taken under microscope.

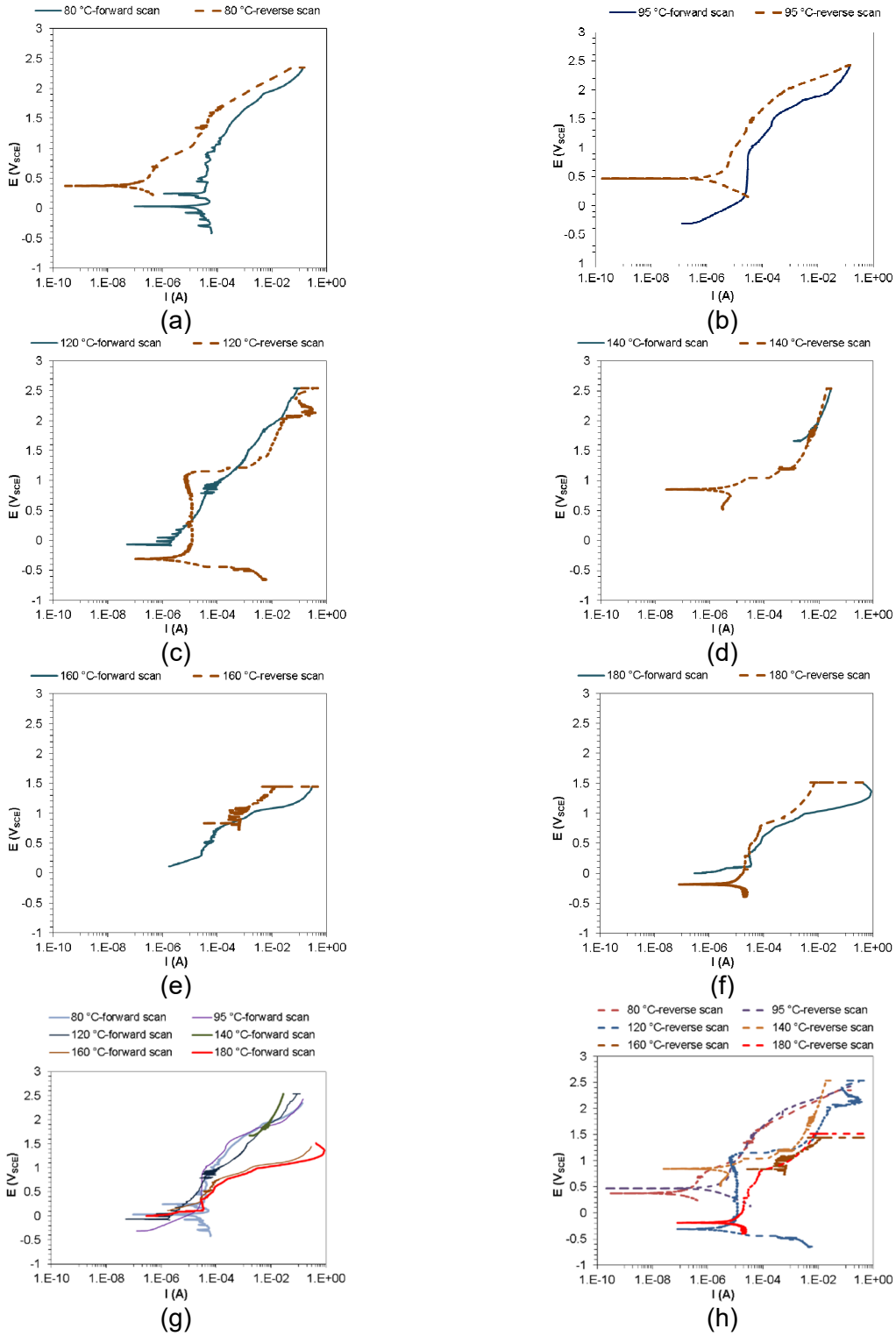

Figure 3-19. Cyclic potentiodynamic polarization of Ti Grade 7 in N_2 deaerated brine (a) 80 °C [176 °F], (b) 95 °C [203 °F], (c) 120 °C [248 °F], (d) 140 °C [284 °F], (e)160 °C [320 °F], (f) 180 °C [356 °F], (g) forward scan, and (h) reverse scan.

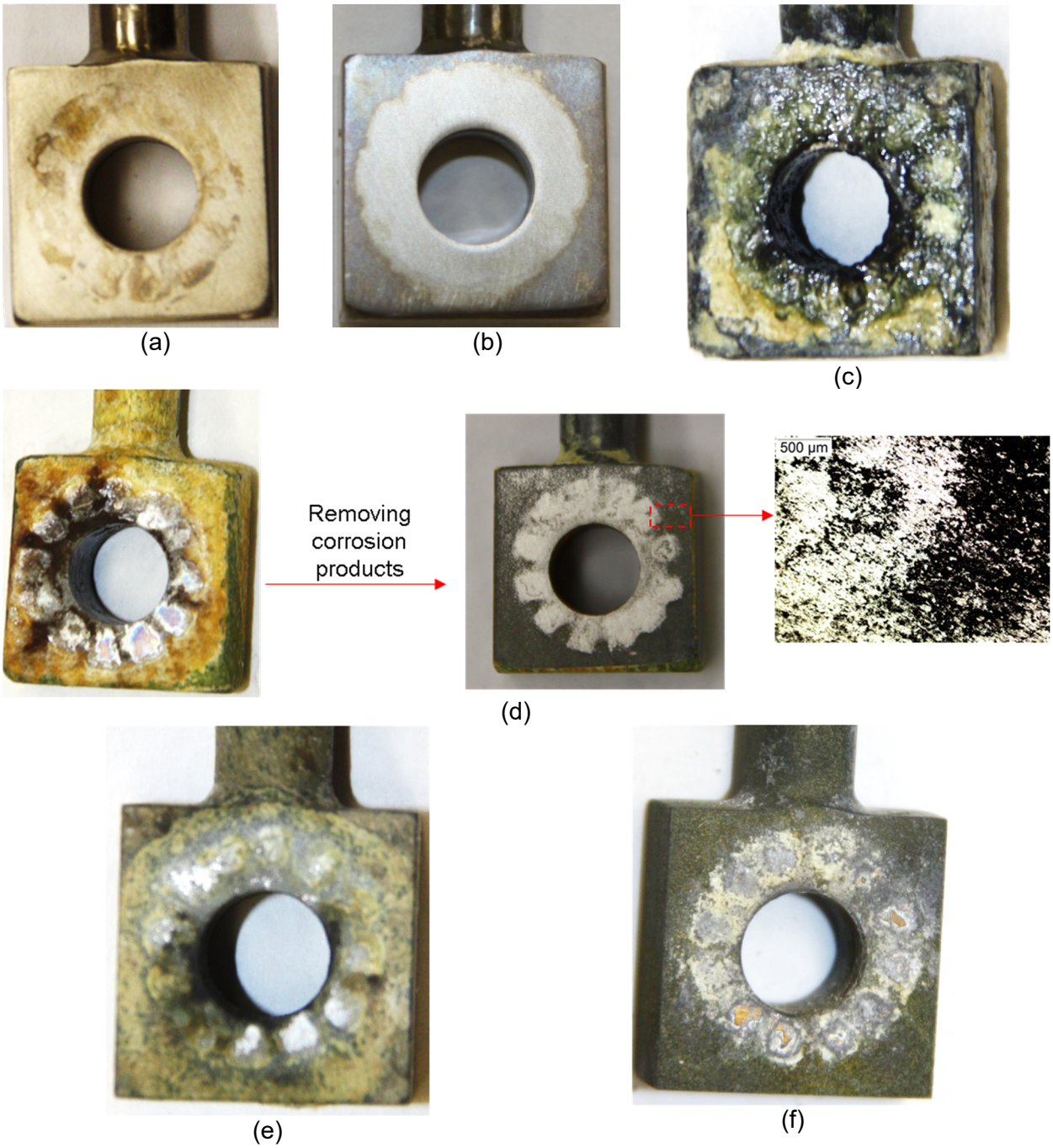

Figure 3-20. Ti Grade 7 coupons after cyclic potentiodynamic polarization in N_2 deaerated brine (a) 80 °C [176 °F], (b) 95 °C [203 °F], (c) 120 °C [248 °F], (d) 140 °C [284 °F], (e)160 °C [320 °F], and (f) 180 °C [356 °F].

The principal observations from Figures 3-19 and 3-20 are summarized as follows.

- During both forward and reverse scans, polarization current at the same polarization potential increased with temperature, indicating that passive dissolution was enhanced by temperature.

- Extensive corrosion was observed at temperatures greater or equal to 120 °C [248 °F]. After removing the corrosion products, the coupon at 140 °C [284 °F] in Figure 3-20(d) exhibited corrosion mostly outside of the crevice, suggesting that the corrosion process was activation controlled (i.e., by electron transfer).

- Except for positive hysteresis observed at 120 °C [248 °F] shown in Figure 3-19(c), no positive hysteresis was observed at other temperatures, indicating strong repassivation after scans up to 2.4, 2.4, 2.5, 2.5, 1.4, 1.5 V_{SCE} at 80 °C [176 °F], 95 °C [203 °F], 120 °C [248 °F], 140 °C [284 °F], 160 °C [320 °F], and 180 °C [356 °F], respectively. This indicates that Ti Grade 7 has strong repassivation tendency, and that the repassivation potentials are higher than the highest applied potentials and corrosion potentials in Figure 3-15(a). This indicates that localized corrosion may not occur in this brine up to 180 °C [356 °F]. This is consistent with the observations in Figure 3-18(b).

3.3.1.5 Cathodic charging in N_2 deaerated brine

Two tests with different surface areas and cathodic charging lengths were performed at 50 °C [122 °F]. Figure 3-21 shows the cathodic charging potential and current and post-charging specimens. In both tests, the charging potential was set at −1.2 V_{SCE}. In the second test, the Ti Grade 7 exposure area was almost one tenth of the first one. The cathodic current density was on the order of 10^{-3} and 10^{-4} A/cm^2. The surface of the post-charging specimen was blackened, but no cracking was observed in specimens from either test. The post-charging specimens at the U-bend apex exposed to the brine were cross sectioned into several pieces without any surface treatment for hydrogen analysis. Two pieces from each specimen along with two control specimens without charging were analyzed for hydrogen content. The hydrogen content is included in Table 3-4. The total amount of absorbed hydrogen from the cathodic charging process was calculated based on the weight of the specimen and the analyzed hydrogen concentration, assuming hydrogen was uniformly distributed in the material. The theoretical amount of hydrogen was calculated using Eq. (3-9) based on the charge and Faraday's Law and is also included in Table 3-4. The hydrogen absorption efficiency was calculated from Eq. (3-9) using the absorbed hydrogen amount divided by the theoretical amount of hydrogen and included in Table 3-4. The computed average efficiency was 0.24 percent and 0.64 percent, respectively for the two tests. These low absorption efficiencies correlate to the lack of cracking in the test. Longer charging time or charging in a more acidic solution or catalyzed surface may facilitate more hydrogen entry.

$$Theoretical\ amount\ of\ hydrogen = \frac{Q}{F} MM \tag{3-9}$$

$$Hydrogen\ absorption\ efficiency\ (\%) = \frac{Amount\ of\ hydrogen\ absorbed}{Theorectical\ amount\ of\ hydrogen} \times 100 \tag{3-10}$$

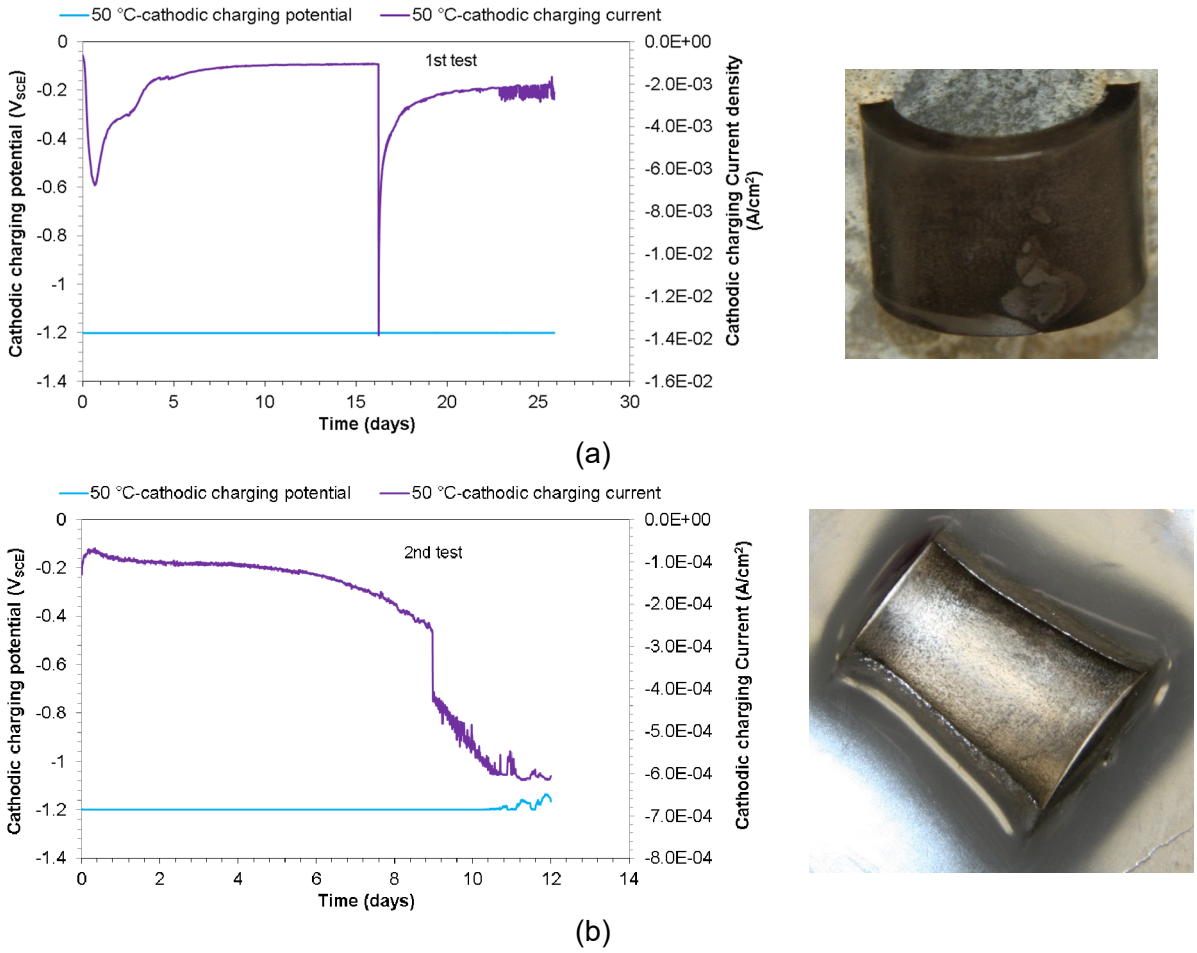

Figure 3-21. Cathodic charging potential and current and post-charging Ti Grade 7 specimens in brine at 50 °C [122 °F] (a) 1st test and (b) 2nd test.

Table 3-4.	**Hydrogen concentration analysis of Ti Grade 7 subject to cathodic charging at 50 °C [122 °F]**						
Time (days)	**Charge, C**	**Surface area, cm^2**	**Weight of specimen, g**	**[Hydrogen], ppm**	**Amount of hydrogen in material, g**	**Theoretical hydrogen from charging**	**Hydrogen absorption efficiency, %**
52	−78,645	16	10.9	153 209	0.0020	0.81	0.24
28	−1,914	1.9	2.55	57 42	0.00013	0.020	0.64
Control specimen				27 39	—		

where

Q = Charge
F = Faraday's constant
MM = Molar mass (1 g/mol for hydrogen)

3.3.2 Titanium Grade 2

3.3.2.1 Corrosion potential in aerated brine

E_{corr} of Ti Grade 2 was only measured at 80 °C [176 °F] for about 25 days, as shown in Figure 3-22. Similar to Figure 3-15(a), E_{corr} increased with time, indicating passivation of the material.

3.3.2.2 Electrochemical impedance spectroscopy in aerated brine

During the E_{corr} measurement shown in Figure 3-22, EIS was performed at Days 1, 6, 12, 18, and 24. The EIS is shown in Figure 3-23. The film became more passive after 1 day and remained steady during the remaining time. Randles circuit shown in Figure 3-17 was used to model the data in the low frequency region. The corrosion parameters and fitting results are summarized in Table 3-5. R_p is similar to the value computed for Ti Grade 7. The calculated general corrosion rate also was negligible.

3.3.2.3 Crevice corrosion experiments exposed to aerated brine

Crevice corrosion tests of Ti Grade 2 were conducted at 80 °C [176 °F], 95 °C [203 °F], and 140 °C [284 °F]. During the test, the Ti Grade 2 crevice specimen was coupled to a large Ti Grade 7 plate as counter electrode. The crevice corrosion current and potential and the post-test crevice coupons are shown in Figure 3-24. Crevice corrosion was not observed at 80 °C [176 °F] over the test duration of 46 days, but corrosion was observed at 95 °C [203 °F] and 140 °C [284 °F]. Section 3.3.1.3 shows that crevice corrosion was not initiated on Titanium Grade 7 at 140 °C [284 °F] in the same solution. This suggests that compared to Ti Grade 7, Ti Grade 2 showed higher localized corrosion susceptibility.

3.3.2.4 Cyclic potentiodynamic polarization in N_2 deaerated brine

Cyclic potentiodynamic polarization of Ti Grade 2 in N_2 deaerated brine was only performed at 80 °C [176 °F], but it was repeated twice. A third test was conducted up to 8 V_{SCE}. Figure 3-25 shows the cyclic potentiodynamic polarization curves of the three tests. The following are key observations:

- There was no corrosion in scans up to 2.8 V_{SCE}.
- Extensive corrosion and positive hysteresis were observed in scans up to 8 V_{SCE}. Corrosion was mostly outside of the crevice, suggesting that the corrosion process was activation controlled.
- The repassivation potential was about 5 V_{SCE}.

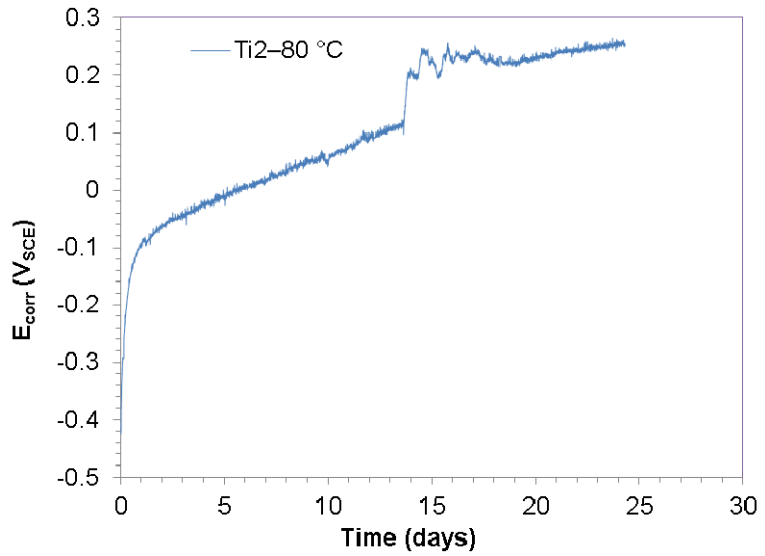

Figure 3-22. E_{corr} of Ti Grade 2 as a function of time in brine at 80 °C [176 °F].

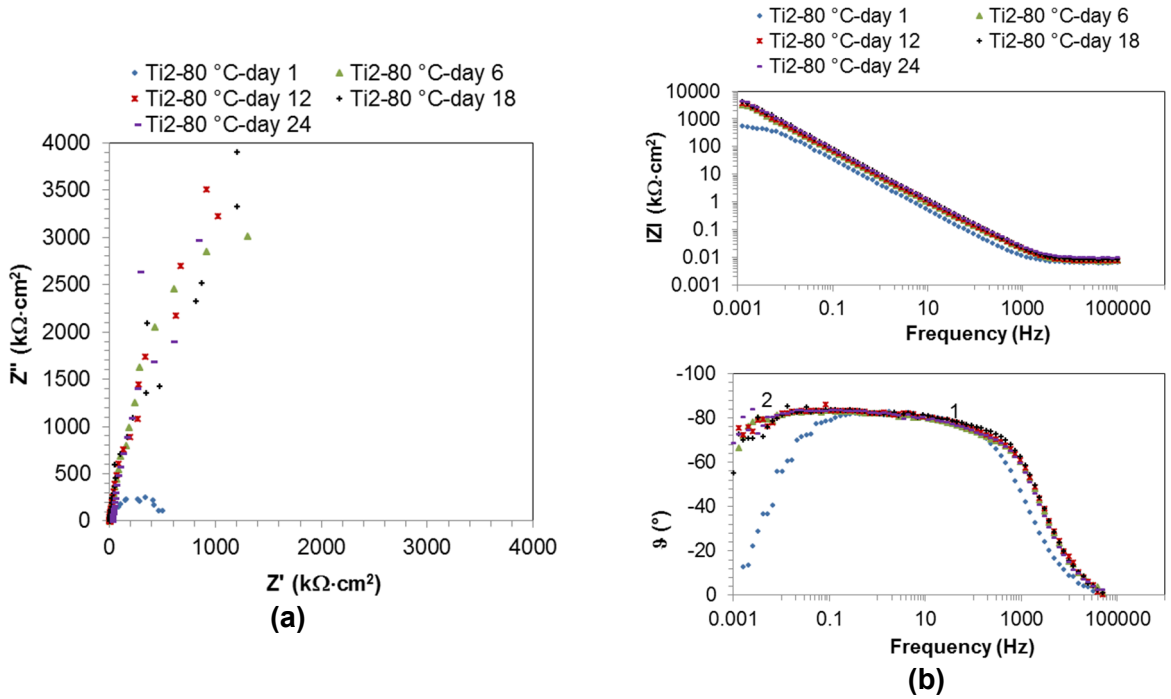

Figure 3-23. EIS of Ti Grade 2 exposed to brine at 80 °C [176 °F] at 1, 6, 12, 18, and 24 days (a) Nyquist plot and (b) Bode plot. The numbers (1 and 2) in the plots are labels indicating curve inflections suggesting two different time constants.

Table 3-5. Corrosion parameters and corrosion rates of Ti Grade 2 derived by fitting EIS to the Randles equivalent circuit					
Temperature	**Time (days)**	**R_p (MΩ·cm²)**	**C_{dl} (µF·cm²)**	**R_s (Ω)**	**Corrosion rate calculated from R_p (nm/y)**
80 °C	1	1	42	0.7	0.424
	6	22	22	0.8	0.011
	12	23	21	0.8	0.010
	18	15	18	0.9	0.016
	24	37	17	1.1	0.006

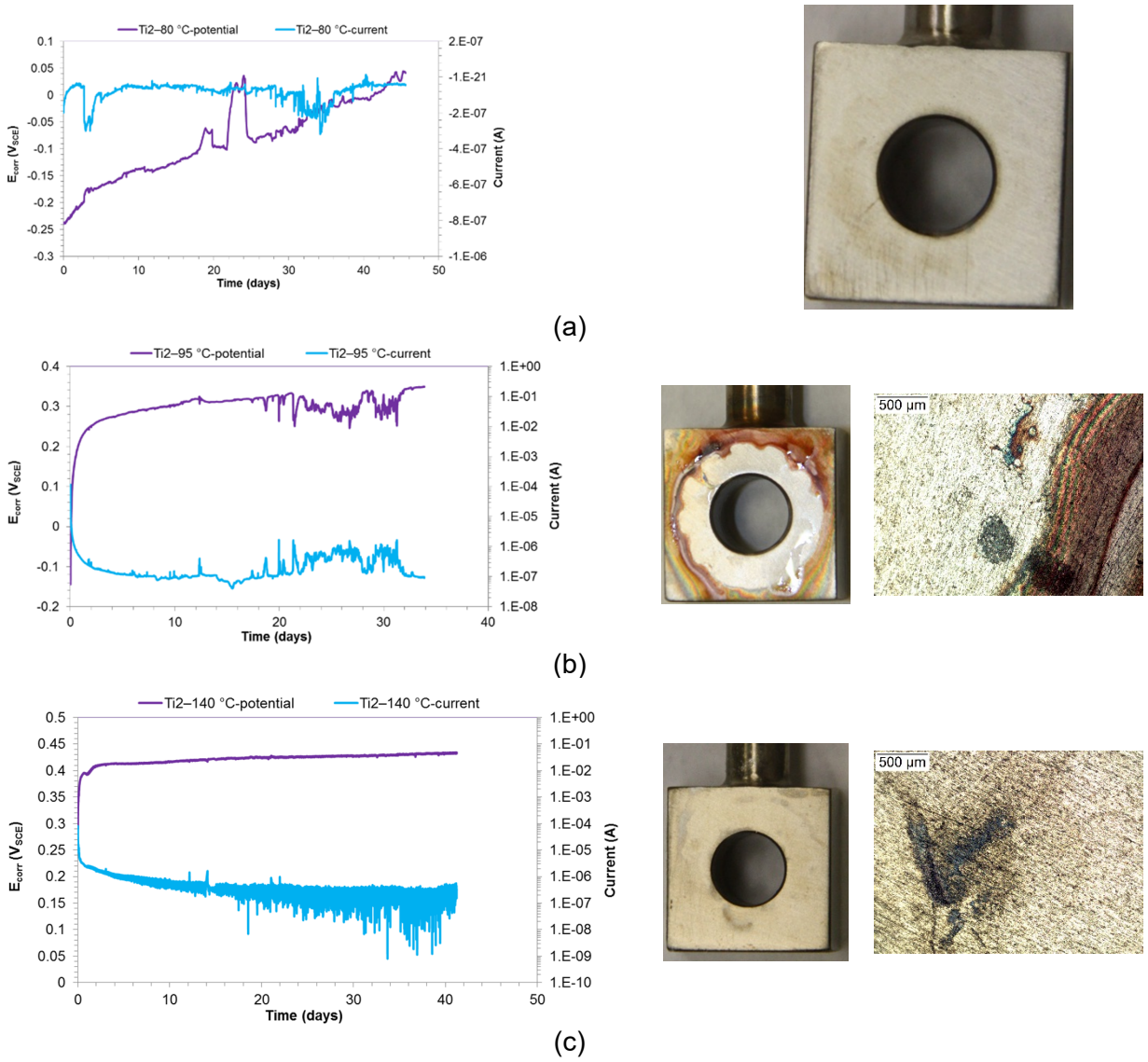

Figure 3-24. Crevice corrosion current and potential of Ti Grade 2 in coupling to Ti Grade 7 at (a) 80 °C [176 °F], (b) 95 °C [203 °F], and (c) 140 °C [284 °F] in brine.

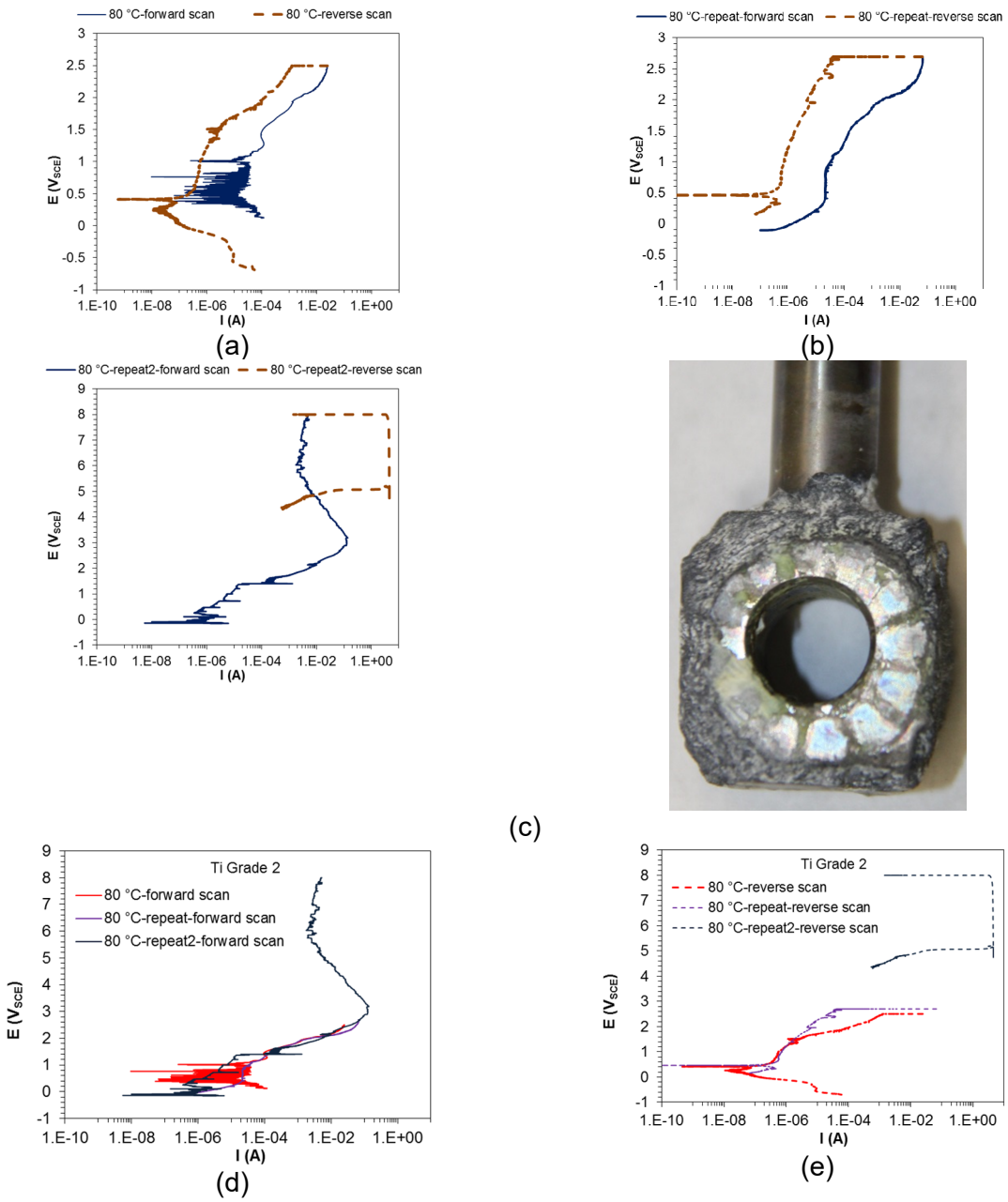

Figure 3-25. Cyclic potentiodynamic polarization of Ti Grade 2 in N_2 deaerated brine (a) 80 °C [176 °F], (b) repeating test at 80 °C [176 °F], (c) repeating test at 80 °C [176 °F] up to 8 V_{SCE} (with a photo of the posttest specimen), (d) forward scan, and (e) reverse scan.

3.3.3 Titanium Grade 29

For Ti Grade 29, only potentiodynamic polarization and hydrogen charging were performed in N_2 deaerated brine. Figure 3-26 shows the cyclic potentiodynamic polarization of Ti Grade 29 in N_2 deaerated brine at 80 °C [176 °F] in comparison to Ti Grades 2 and 7. At 2.8 V_{SCE}, the polarization current increased more quickly than Ti Grades 2 and 7.

Figure 3-27 shows the cathodic charging potential and current of Ti Grade 29 specimen in brine at 50 °C [122 °F]. The charging potential was about −1.2 V_{SCE}. The current fluctuated with

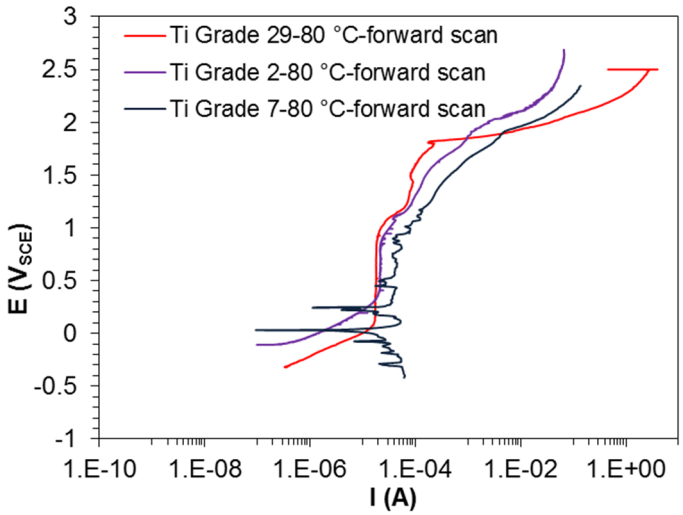

Figure 3-26. Cyclic potentiodynamic polarization of Ti Grade 29 in N_2 deaerated brine at 80 °C [176 °F] in comparing to Ti Grades 2 and 7.

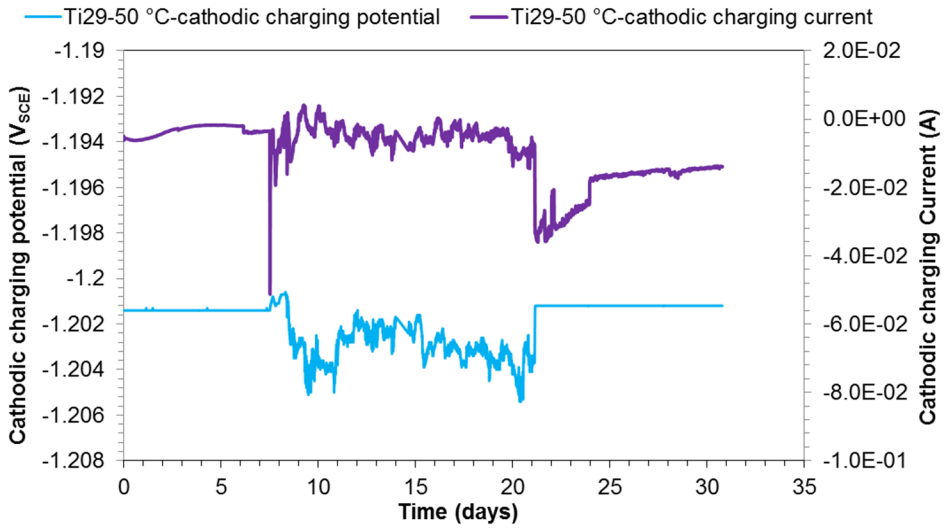

Figure 3-27. Cathodic charging potential and current of Ti Grade 29 specimen in brine at 50 °C [122 °F].

time. Two specimens were cut from the charged coupon. The hydrogen concentration of the specimen cut from the charged coupon was measured to be 328 and 333 ppm, which is higher than the blank (untested material), but no cracking was observed.

3.3.4 Discussion

Ti Grade 2 is a commercially pure Ti without any alloying element. Ti Grade 7 has palladium (Pd) as noble element incorporated into its primary α-phase grains. This work showed that both Ti Grades 2 and 7 maintained similar levels of high passivity and exhibited negligible general corrosion in brine at 80 °C [176 °F]. This suggests that the Pd addition in Ti Grade 7 may not have much effect on passivity, and that the passivity in the brine may be dominated by the oxide film and the phase structure. However, the comparison was only conducted at one

temperature. Passivity of Ti Grade 2 at temperatures higher than 80 °C [176 °F] may be different: Figures 3-19 and 3-20 suggest that corrosion can be enhanced by increased temperature. Therefore, the passivity and general corrosion rates of Ti Grades 2 and 7 could differ at higher temperatures. Additional tests will be needed to substantiate the effects of alloy composition over a broader temperature range. Figure 3-26 shows that the polarization current of Ti Grade 29 increased more quickly than for Ti Grades 2 and 7. This could be mainly because of the difference in microstructure. Ti Grade 29 has both α and β phases, whereas, Ti Grades 2 and 7 are single α-phase material. The grain boundaries in Ti Grade 29 may have served as higher energy sites for passive dissolution.

Comparison of crevice corrosion tests in this work shows that Ti Grade 2 was susceptible to crevice corrosion in the brine at elevated temperatures, but it was not observed in Ti Grade 7. The limited number of tests suggests that addition of palladium (Pd) increases the crevice corrosion resistance. One mechanism to explain the increased crevice corrosion resistance is schematically illustrated in Figure 3-28. For the unalloyed Ti, the polarization curve for the cathodic reaction (H^+/H_2) intersects the anodic polarization curve in the active region. This suggests that crevice corrosion is possible for unalloyed Ti. However, the addition of Pd in Ti forms intermetallics, which can catalyze the cathodic reaction. As a result, the intermetallics shift the alloy corrosion potential in the positive direction, where oxide film passivation is maintained and crevice corrosion resistance is increased. Cathodic charging of Ti Grade 7 shows that this material absorbed hydrogen from cathodic charging, but the absorption efficiency was very low, which also could be the result from the addition of Pd. However, no test was performed on Ti Grade 2 under similar conditions. Therefore, additional tests will be needed to tell if the low hydrogen absorption efficiency and high hydrogen induced cracking resistance are associated with the Pd addition. Limited testing performed on Ti Grade 29 provided little information on how the co-existence of α and β phases affects hydrogen absorption and hydrogen induced cracking resistance in the brine. Ti Grade 12 (Ti-0.3Mo-0.8Ni) was a candidate waste container material for a rock salt repository (Ahn et al., 1984). It may be appropriate to conduct a comparison test to better understand how the intermetallic particles affect the corrosion performance in this brine.

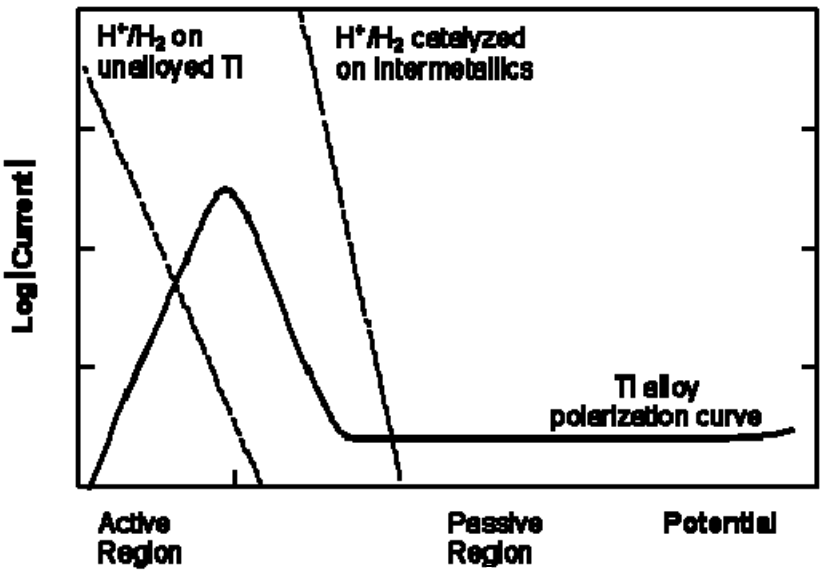

Figure 3-28. Schematic illustrating the polarization curve for Ti and its relationship to the cathodic polarization curves for proton reduction on Ti Grade 2 and on a Ti alloy containing a catalytic alloying element such as Pd.

4 SUMMARY

The objective of this study was to evaluate the corrosion resistance of three candidate waste package materials for high level radioactive waste (HLW) containment in a potential deep geologic repository. Solution contacting the waste package could be anoxic after tens or hundreds of years or in a salt formation where the chemical solution could be an oxic brine in the early stages after repository closure. Because of the decay heat from the HLW, the temperature around the waste package is expected to be elevated. The work focused on (i) examining the possibility of hydrogen induced cracking of carbon steel under static loading in simulated granitic groundwater; (ii) evaluating copper (Cu) corrosion in simulated granitic groundwater and repeating the evaluation of the effects of chloride (Cl^-) on Cu corrosion at 50 °C [122 °F] to corroborate previous results; and (iii) evaluating titanium (Ti) passivity, localized corrosion resistance, and hydrogen induced cracking in a synthetic brine with a composition similar to a brine found near the Waste Isolation Pilot Plant (WIPP) site. The results are summarized as follows.

- No cracking was observed under cathodic charging of carbon steel over the test duration of 3 months under a static loading condition in simulated granitic groundwater, even after the solution was acidified to pH 2, temperature was elevated, and exposure surface was creviced to facilitate hydrogen entry.

- The corrosion potential (E_{corr}) of Cu immersed in solutions decreased with increasing Cl^- concentrations. Under potentiodynamic polarization, Tafel slopes decreased and exchange current density increased with increasing Cl^- concentration. The electrochemical impedance spectroscopy (EIS) data varied in solutions with different Cl^- concentrations. It was consistently observed that Cl^- plays a significant role in enhancing corrosion of copper in solutions with extremely low O_2 concentrations. Higher temperature and higher Cl^- concentration could have depolarized the anodic reaction, resulting in lower E_{corr} values and potentially larger i_{corr}. The Cu corrosion process in these solutions with extremely low O_2 concentrations could be mostly controlled by mass transport. Additional tests are needed to further understand the cathodic reaction and the corrosion products.

- Passivity of Ti materials depends on alloying elements, microstructure, and environmental conditions. Ti Grade 7 exhibited high passivity, negligible general corrosion, and strong repassivation up to 180 °C [356 °F] in brine. This material also exhibited high crevice corrosion resistance and very low hydrogen absorption efficiency. Ti Grade 2 showed a similar level of general corrosion resistance as Ti Grade 7 at 80 °C [176 °F], but it is susceptible to crevice corrosion. Ti Grade 29 showed lower passivity in the same brine compared to Ti Grades 2 and 7 at 80 °C [176 °F]. Additional tests are needed to further understand how noble alloying elements such as Pd and ruthenium (Ru) and microstructure such as β-phase and intermetallic particles affect the passivity, localized corrosion resistance, and hydrogen induced cracking resistance in this brine representing solutions in salt formations.

5 REFERENCES

Ahn, T.M., B.S. Lee, and P. Soo. “Identification of Crevice Corrosion in Titanium Alloy Ti Code-12 in Rock Salt Brine at 150° C.” ASTM STP 830 Titanium and Zirconium in Industrial Applications, Edited by R. T. Webster and C. S. Young, pp. 159–174. 1984.

Betova, I., M. Bojinov, and C. Lilja. “Long-Term Interaction of Copper with a Deoxygenated Neutral Aqueous Solution.” *Journal of the Electrochemical Society.* Vol. 160. pp. C49–C58. 2013.

Dunn, D.S., O. Pensado, Y.-M. Pan, R.T. Pabalan, L. Yang, X. He, and K.T. Chiang. “Passive and Localized Corrosion of Alloy 22—Modeling and Experiments.” San Antonio, Texas: Center for Nuclear Waste Regulatory Analyses. ADAMS Accession Number ML050700371. 2005.

Eriksen, T.E., P. Ndalamba, and I. Grenthe. “On the Corrosion of Copper in Pure Water.” *Corrosion Science*. Vol. 29. pp. 1,241–1,250. 1989.

He, X. and T. Ahn. “Effects of Chloride on Copper Corrosion.” Washington, DC: U.S. Nuclear Regulatory Commission. 2018.

He, X. and T. Ahn. “Effects of Chloride on Copper Corrosion and Cathodic Charging of Carbon Steel for Nuclear Waste Disposal Application.” ML17304A897. Washington, DC: U.S. Nuclear Regulatory Commission. 2017a.

He, X. and T. Ahn. “Experiments on Corrosion of Copper and Carbon Steel Waste Containers—Progress Report for Fiscal Years 2015 and 2016.” ML17003A453. Washington, DC: U.S. Nuclear Regulatory Commission. 2017b.

He, X., T. Ahn, and J. McMurry. “Literature Review and Experiments on Waste Package Corrosion—Copper and Carbon Steel.” ML16014A269. Washington, DC: U.S. Nuclear Regulatory Commission. 2015.

Hedin, A., A.J. Johansson, C. Lilja, M. Boman, P. Berastegui, R. Berger, and M. Ottosson. “Corrosion of Copper in Pure O_2-Free Water?” *Corrosion Science*. Vol. 137. pp. 1–12. 2018.

Kear, G., B.D. Barker, and F.C. Walsh. “Electrochemical Corrosion of Unalloyed Copper in Chloride Media—A Critical Review.” *Corrosion Science*. Vol. 46. pp. 109–135. 2004.

King, F. “Container Materials for the Storage and Disposal of Nuclear Waste.” *Corrosion*. Vol. 69. pp. 986–1,011. 2013.

Kursten, B. and R. Gaggiano. “SCC Study of Mild Steel Welds Exposed to Concrete Pore Water under Anoxic Conditions.” Proceedings of Annual Corrosion Conference. NACE International. Houston, Texas. 2018.

Simpson, J.P. and R. Schenk. “Hydrogen Evolution from Corrosion of Pure Copper.” *Corrosion Science*. Vol. 27. pp. 1,365–1,370. 1987.